Imperial College London
Department of Theoretical Physics

Topological Quantum Computing: Fabry-Pérot Interferometers as a Means of Implementing a Quantum NOT-Gate

Paul D. Gorman

September 25^{th} 2009

Supervised by Dr.T.Rudolph
& Dr.J.Slingerland

Submitted in part fulfilment of the requirements for the degree of
Masters in Theoretical Physics of Imperial College London
and Diploma of Imperial College London

Acknowledgements:

I'd like to thank Tez and Joost for supervising this dissertation.

"...without thought or conscious desire, might not things external to ourselves vibrate in unison... atom calling onto atom, in secret love of strange affinity?"

- Oscar Wilde

ABSTRACT:

In this paper we explain the basics of Topological Quantum Computing, show that Interferometry is useful in analyzing anyon models, discuss how the 3-point Fabry-Pérot type Interferometer can be used as a quantum NOT-gate, and construct the Unitary and Density Matrices describing anyon interactions within it.

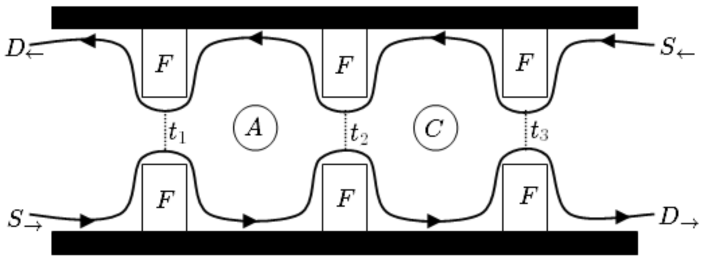

Contents

1 Introduction

This paper constitutes an Introduction to the methods of Topological Quantum Computing and an application of these methods to different types of interferometers.

Chapter 1 is a basic introduction to Topological Quantum Computing. For a general introduction to Quantum Computing see [1, 2].

Chapter 2 deals with the general physics and diagrammatic methods needed to understand chapter 3 and other papers on the subject.

Chapter 3 deals with detailed explanations of the calculations done in [3, 4] concerning the 2-point Fabry-Pérot and Mach-Zehnder interferometers. Where sections 3.2.2 and 3.2.3 consist of original calculations applying the methods of [3, 4] to the 3-point Fabry-Pérot Interferometer described in [5].

1.1 Introduction to Topological Quantum Computing

A Topological Quantum Computer [TQC] is a condensed matter system whose excitations, satisfying non-abelian braiding statistics, can be exploited to perform inherently error-free quantum computations [6].

One of the fundamental differences between a TQC and non-TQC lies in the locality of the qubits[1]. Non-TQCs have local qubits and perform *local* operations on them, which makes them susceptible to errors caused by *local* perturbations (interactions with the environment). TQC store qubits in a non-local manner and the operations are non-local , which makes them resilient to local perturbations [Sec. 2.3].

TQC are also naturally immune to errors introduced by unitary gate operations, as braiding operations naturally take on a discrete set of values. The standard example of how an error is introduced when one is dealing with spin-based qubits is that, in the task of performing a rotation of 90 degrees a rotation of 89.99 or 90.01 will occur, creating a small error. Since TQC operations are performed by taking quasiparticles [Sec. 2.1] around each other, no error will

[1] The quantum equivalent of standard computational bits 0 & 1, which is a superposition of the the two states.

be introduced by a quasiparticle being taken partially around another unless it changes the topological class of the link formed by the particle trajectories [Sec. 3.1]. So, the only errors we must concern ourselves with are those that might cause us to form the wrong link, resulting in the wrong calculation.

We will see in the following sections that there remain many barriers to the implementation of a TQC, including: identifying an anyonic model capable of universal quantum computation, creating and controlling anyons, and the construction of large scale architectures for a quantum computer.

2 The Tools of Topological Quantum Computing

Discussed in this section is the necessary information to understand the calculations of Chapter 3. Each section follows from the previous so that the information is built up in the correct manner.

Since the next few sections have multiple overlapping sources I have left most referencing to the end of each section.

2.1 Fractional Quantum Hall Effect

The Hall Effect [7] is observed when an electric current flows through a conductor in an orthogonal magnetic field. The magnetic field exerts a transverse force on the charge carriers (electrons, electron-holes etc), pushing them to one side of the conductor. There results a measurable voltage between the two sides of the conductor due to the buildup of charge balancing the magnetic influence.

The quantum-mechanical version of the Hall Effect [8–10], only observed in two-dimensional systems, occurs at low-temperatures (∼30mK)[1] and in the presence of strong magnetic fields(∼20T), when the Hall conductivity σ_{XY} takes on quantized values. In general

$$\sigma_{XY} = \nu \frac{e^2}{h} \tag{2.1}$$

where h is Planck's constant, e is the electric charge and ν is known as the *Filling Factor*. The filling factor is defined by the ratio of electrons to magnetic flux quanta, it specifies the Quantum Hall Effect as either Fractional or Integer. The integer case, $v \in \mathbb{N}$, is well understood in terms of non-interacting electrons in a magnetic field.

We are especially interested in the instances when the Hall resistance does not rise linearly with the applied magnetic field, but instead exhibits plateaux. This occurs when the current moves perpendicular to the applied voltage, or put another way, when the Fermi energy lies in a gap of the density of states.

[1]There exists some evidence of FQHE at higher temperatures [11]

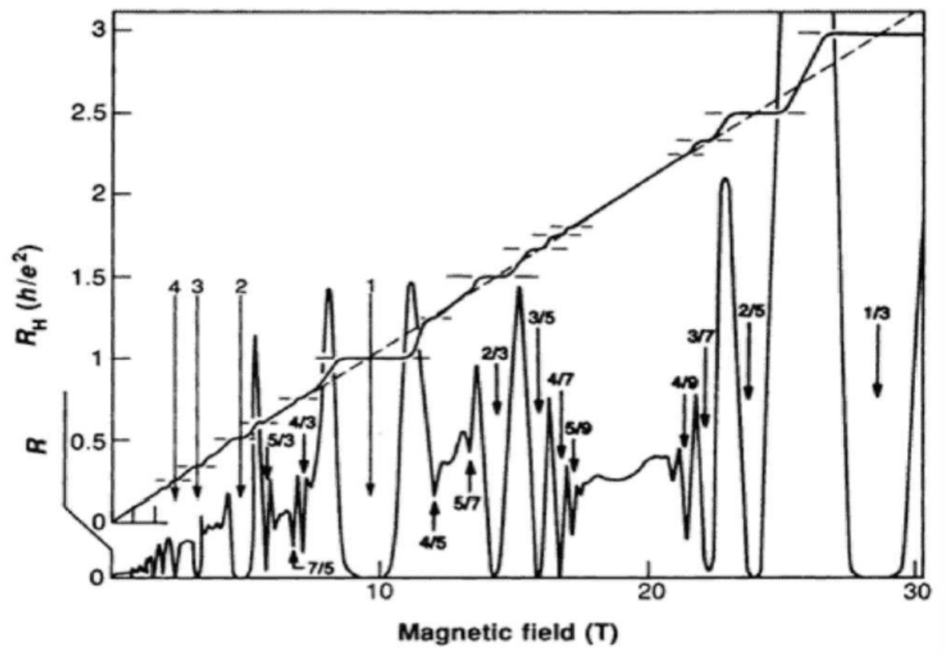

Figure 2.1: Experimental results for hall resistance, from [12]

At each plateau the electrons form an incompressible fluid state with interesting localized excitations. The quasiparticles (and quasiholes[2]) that appear at fractional plateaux exhibit exotic properties, such as having a fraction of the charge of the electron and are even predicted to be *non-abelian* in some cases. It is these non-abelian cases that we are especially interested in experimentally, as they may correspond to non-abelian Anyons; this is discussed in Section 2.2.

To further understand the effect, consider a system of free particles of charge $-e$ and mass m in two dimensions, under the influence of a magnetic field $\mathbf{B} = (0, 0, B)$. Ignoring the spin of the electrons, the single particle Hamiltonian for the system is

$$H = \frac{1}{2m}\left((p_x - \tfrac{e}{c}A_x)^2 + (p_y - \tfrac{e}{c}A_y)^2\right) \tag{2.2}$$

where $\mathbf{A}$ is a vector potential which gives rise to the required magnetic field. We work in the gauge that specifies

$$\mathbf{A} = \left(-\tfrac{B}{2}y, \tfrac{B}{2}x, 0\right) \tag{2.3}$$

[2]If these excitations correspond to a local peak in the electron density, then they are referred to as *quasiparticles*. If they correspond to a local dip in the electron density, then they are referred to as *quasiholes*.

Translated into dimensionless complex coordinates, $z = \frac{x+iy}{l}$, where $l = \sqrt{\frac{\hbar c}{eB}}$ and the Hamiltonian H and the angular momentum $L = xp_y - yp_x$ (with some work) become

$$\begin{aligned} H &= \tfrac{1}{2}\tfrac{\hbar eB}{mc}\left(-4\partial_z\partial_{\overline{z}} - \partial_s + \overline{z}\partial_{\overline{z}} + \tfrac{1}{4}z\overline{z}\right) \\ L &= \hbar(z\partial_z - \overline{z}\partial_{\overline{z}}) \end{aligned} \tag{2.4}$$

Similarly to the usual solution of the Harmonic oscillator, we find the operators

$$\text{Creation operators} \begin{cases} a^\dagger = \partial_z - \frac{\overline{z}}{4} \\ b^\dagger = \partial_{\overline{z}} - \frac{z}{4} \end{cases} \tag{2.5}$$

$$\text{Annihilation operators} \begin{cases} a = -\partial_{\overline{z}} - \frac{z}{4} \\ b = -\partial_z - \frac{\overline{z}}{4} \end{cases} \tag{2.6}$$

where $a, a^\dagger$ commute with $b, b^\dagger$ and

$$[H, a^\dagger] = \frac{\hbar eBa^\dagger}{mc}, \qquad [H, b^\dagger] = 0 \tag{2.7}$$

By solving

$$a\psi_{0,0} = b\psi_{0,0} = 0 \tag{2.8}$$

we find the *lowest weight* ground state $\psi_{0,0}(z, \overline{z}) := e^{-z\overline{z}/4}$. Applying $a^\dagger$ and $b^\dagger$ to this state, we obtain a basis of eigenstates of H

$$\psi_{m,n}(z) = \left(\partial_{\overline{z}} - \tfrac{z}{4}\right)^m \left(\partial_z - \tfrac{\overline{z}}{4}\right)^n e^{-z\overline{z}/4} \tag{2.9}$$

The corresponding energy levels

$$E_n = \frac{\hbar eB}{mc}\left(n + \tfrac{1}{2}\right) \tag{2.10}$$

are known as *Landau Levels* [13] and are independent of m, hence infinitely degenerate. Each Landau level can be distinguished by its angular momentum. From

$$L\psi_{0,0} = 0 \tag{2.11}$$

and the commutation relations

$$[L, a^\dagger] = \hbar a^\dagger, \qquad [L, b^\dagger] = -\hbar b^\dagger \tag{2.12}$$

we have that

$$L\psi_{m,n} = \hbar(m-n)\psi_{m,n} \tag{2.13}$$

The angular momentum eigenstates in the first Landau level are just the functions $z^m e^{-z\bar{z}/4}$, with eigenvalues $m\hbar$. Confining the sample results to a finite region in the plane results in a loss of the infinite degeneracy of the Landau levels. Each single-particle state then takes a surface area $\frac{hc}{eB} = l^2$, so that each Landau level contains $\frac{eBA}{hc}$ states (Where A is the surface area of the sample). Thus the number of states in a Landau level equals the number of fundamental flux quanta $\frac{e}{hc}$ that pierce the sample.

The Fractional Quantum Hall Effect (FQHE) depends essentially on the repulsive interactions between all the electrons in the system. To see where the values for the filling fractions come from we look at Laughlin's variational wave functions for a system of N electrons on a disc [9]. Starting at the ground state, the wave functions are

$$\psi_N^m(z_1, ..., z_N) = \prod_{i<j}(z_i - z_j)^{2m+1} e^{-(\frac{1}{4}\sum_i z_i \bar{z}_i)} \tag{2.14}$$

where z_k are complex coordinates for the electrons and $m \in \mathbb{Z}$. From this, we can read off the the maximal angular momentum for a particle. A simple way to find the filling fraction is by considering the fact that since the electrons fill the sample space, the highest occupied single article angular momentum state must also be the highest Landau level. Whereas the maximal angular momentum for a single particle is just the maximal power of a single z_k, which is $(2m+1)(N-1)$. The first Landau level contains $(2m+1)N$ states, so for N electrons, we have a filling fraction $\nu = \frac{1}{2m+1}$. [14–16]

The FQH plateaux, filling fractions, and the fractional charge of the quasi-particles in the first landau level are well described by Laughlin states, and the Abelian hierarchy states constructed over them [17–19].

The discovery of the FQHE in 2-DEG (two-dimensional electron gases), in a strong magnetic field, indicated that the effect occurs exclusively at Landau level filling factors with *odd* denominators [20, 21]. Also important is the fact that the electron gas (under the right specific conditions:high quality material with a low carrier concentration etc) condenses into a remarkable system with liquid-like properties, which we call a *Fractional Quantum Hall Liquid* (FQHL). The discovery of FQHE in an *even* denominator filling factor $\frac{5}{2}$ in the second landau level [22] was the first indication that not all fractional quantum Hall states fit the Abelian hierarchy.

Using Conformal Field Theory the Moore-Read Pfaffian wavefunction was constructed

$$\Psi_{Pf} = Pf\left(\frac{1}{z_i - z_j}\right)\prod_{i<j}(z_i - z_j)^m e^{-\sum_i |z_i|^2/4l_0^2} \tag{2.15}$$

which, for even m, describes an even-denominator quantum Hall state in the lowest Landau level. It was suggested by Moore and Read [23] that its quasiparticle excitations would exhibit*non-Abelian statistics*, which correspond to *non-abelian* anyons.

2.2 Anyons

In our three spatial dimensions we live with fermions and bosons, conforming to Fermi-Dirac and Bose-Einstein statistics respectively. In 1977 *Leinaas and Myrheim* [24] (and later *Wilczek*) realized that if we were to live in a (2+1)-dimensional Flatland[3] we would find ourselves in the company of quasiparticles known as *Anyons*, a term coined by *Wilczek* in 1982. These anyons obey neither Fermi-Dirac nor Bose-Einstein statistics, but are instead governed by a third set of statistics usually referred to as fractional or anyonic statistics.

To understand their behaviour we must look at the behaviour of multiparticle states under the exchange of particles. For a particular pair of bosons $|\psi_1\psi_2\rangle$ under interchange, we have the symmetric relation $|\psi_1\psi_2\rangle = +|\psi_2\psi_1\rangle$. And for a particular pair of fermions $|\psi_1\psi_2\rangle$, we have the antisymmetric relation $|\psi_1\psi_2\rangle = -|\psi_2\psi_1\rangle$. However, for a particular pair of Anyons we have the relation $|\psi_1\psi_2\rangle = e^{i\theta}|\psi_2\psi_1\rangle$, meaning that they can acquire *any* phase when interchanged. Notice that for $\theta = \pi, 3\pi...$, we have Fermi-Dirac statistics and for $\theta = 0, 2\pi...$, we have Bose-Einstein statistics.

Consider, for a moment, the symmetry properties of an N-particle wavefunction $|\psi\rangle$ on a D-dimensional manifold. In general, under an arbitrary permutation Π, the Hamiltonian of the system remains invariant, but the wavefunction transforms as

$$\Pi : |\psi\rangle \to U(\Pi)|\psi\rangle \tag{2.16}$$

where $U(\Pi)$ are matrices representing the symmetry group of the permutation Π. For our D-dimensional, N-particle system, we have the configuration space M_N^D. The fundamental group $\Pi_1(M_N^D)$ gives the symmetry group of the permutation, and thus the symmetry properties depend on the configuration space topology. In general the configuration space M_N^D is not simply connected, because indistinguishable particles are allowed to coincide, meaning that the fundamental group is non-trivial and depends on D [25, 26]. In $D \geqslant 3$ spatial

[3]For cultural reference see *Flatland: A Romance of Many Dimensions* by *A.Square*

dimensions, the fundamental group is isomorphic to the permutation group of N-objects:S_N

$$\Pi_1(M_N^D) \backsimeq S_N, \quad D \geqslant 3. \tag{2.17}$$

However, in $D = 2$ spatial dimensions it is isomorphic to the braid group of N-strands B_N

$$\Pi_1(M_N^2) \backsimeq B_N \tag{2.18}$$

(Note: in $D = 1$ spatial dimensions quantum statistics is not well defined since particle interchange is not possible without one particle passing through another.) The irreducible representations of S_N & B_N give the matrices $U(\Pi)$, thus they govern the transformation properties of the wavefunction. We therefore only expect to observe anyonic behaviour in systems of two spatial dimensions where the symmetry properties of $|\psi\rangle$ are described by the braid group B_N, which fully captures all the long range interactions in a (2+1)-D system.

2.3 Braiding

The structure of the braid group B_N can be intuitively visualized by considering the worldline trajectories of our quasiparticles as strands with time in the direction of the arrow and particles $1, ..., N$ along the x-axis.

B_N is generated by $N-1$ generators $\sigma_1 ... \sigma_{N-1}$. Where the operation σ_i indicates a counter-clockwise (or left over right) interchange of the ith and $(i+1)$th particles (strands) as indicated in Fig.2.2. For our particle this results in an acquired $e^{in\theta}$phase, where n is the number of times that one particle winds another (minus the number of times that it winds the other way). The inverse σ_i^{-1} indicates a clockwise interchange, and the corresponding acquired phase $e^{-in\theta}$. And gives the relation

$$(\sigma_i)^{-1}\sigma_i = \sigma_i(\sigma_i)^{-1} = e, \qquad e^{-in\theta}.e^{in\theta} = 1 \tag{2.19}$$

where e is the identity element of the braid group.

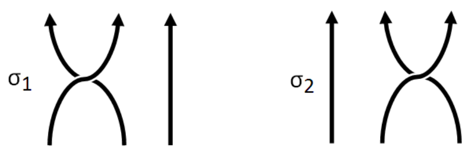

Figure 2.2: σ_1: the operation of interchanging the particles at 1 & 2 by moving 1 counter-clockwise around 2. σ_2: the operation of interchanging particles 2 & 3 by moving 2 counter-clockwise around 3

The braid group has two constraints, the first constraint

$$\sigma_i \sigma_j = \sigma_j \sigma_i, \quad |i-j| \geq 2, \tag{2.20}$$

is an algebraic expression of Fig. 2.3 and Fig. 2.4, and of the fact that $\sigma_i^2 \neq e$,

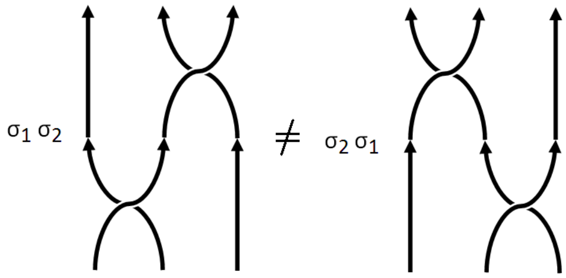

Figure 2.3: $\sigma_1\sigma_2 \neq \sigma_2\sigma_1$

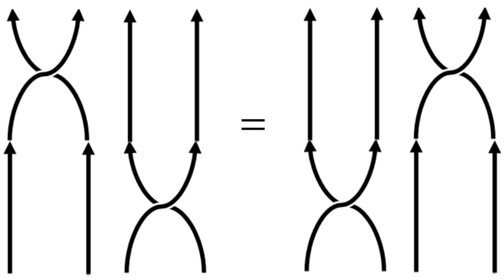

Figure 2.4: $\sigma_1\sigma_3 = \sigma_3\sigma_1$

in contrast to the permutation group S_N where $\sigma_i^2 = e$. This is important to note as it leads to the fact that there exists no theorem constraining the dimensionality of the irreducible representations of the braid group; $B_N, N \geq 3$ is a *non-abelian* infinite group. It is this richness of the braid group that allows quantum computation through quasiparticle braiding.

The second constraint

$$\sigma_i \sigma_{i+1} \sigma_i = \sigma_{i+1} \sigma_i \sigma_{i+1} \tag{2.21}$$

is the algebraic expression of the Yang-Baxter relation shown in Fig. 2.5.

Non-abelian braiding statistics is associated with higher dimensional representations of the braid group, which occur when there is a degenerate set of g states with particles at fixed positions $x_1 ... x_N$. Defining an orthonormal basis $\psi_\alpha, (\alpha = 1, 2, ..., g)$ of these degenerate states, an element of the braid group σ_i

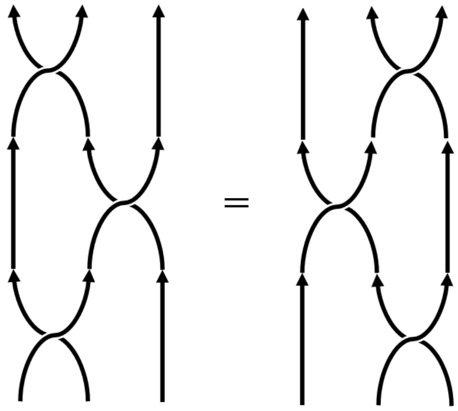

Figure 2.5: Yang-Baxter relation: $\sigma_i\sigma_{i+1}\sigma_i = \sigma_{i+1}\sigma_i\sigma_{i+1}$

is represented by a g x g unitary matrix $\rho(\sigma_i)$, which defines a unitary transformation within the subspace of degenerate ground states.

$$\psi_\alpha \to [\rho(\sigma_i)]_{\alpha\beta}\psi_\beta \tag{2.22}$$

The particles are said to obey non-abelian braiding statistics if

$$[\rho(\sigma_1)]_{\alpha\beta}[\rho(\sigma_2)]_{\beta\gamma} \neq [\rho(\sigma_2)]_{\alpha\beta}[\rho(\sigma_1)]_{\beta\gamma} \tag{2.23}$$

which, in general, will result in non-trivial rotations of the Hilbert space.

The topological nature of these interactions has two unusual consequences. Firstly, the phase acquired is independent of the path travelled, depending only on the number and order of interchanges, making the phase immune to minor fluctuations in the worldline. At low energies, it is essentially true that the only way to make non-trivial unitary operations is by braiding quasiparticles, which is equivalent to saying that no local perturbations can have non-zero matrix elements within this degenerate space. Secondly, because there are no particles mediating the interaction it is a non-local effect, meaning that it persists even with a large spatial separation. [27–29]

2.4 Fusion

Fusion is the formation of a different type of anyon by bringing two anyons together, though not necessarily a bound state as no such bound state may exist, it is enough to simply bring two anyons close together while all other anyons are much further away. For example, consider a system of abelian anyons with braiding statistics θ, a bound state of two such anyons will have braiding statistics 4θ. We then consider the two anyons to be a single anyon whose quantum numbers are obtained by combining the quantum number of the two particles.

So, if there are $\theta = \pi/m$ anyons in a system, then we must also consider there to be

$$\theta = 4\frac{\pi}{m}, \quad 9\frac{\pi}{m}, \quad ..., \quad (m-1)^2\frac{\pi}{m} \tag{2.24}$$

anyons in the system. With

$$\theta = (m-1)^2\frac{\pi}{m} = -\frac{\pi}{m} \tag{2.25}$$

for m even, and

$$\theta = (m-1)^2\frac{\pi}{m} = \pi - \frac{\pi}{m} \tag{2.26}$$

for m odd, since the statistics parameter is only well defined up until $\theta = 2\pi$.

Combining a $-\pi/m$ particle and a $+\pi/m$ particle results in a particle with statistics $\theta = 0$ (boson). Such a particle is as good as the absence of a particle and as such is typically called the *'trivial particle'* or simply the *'vacuum'*. We will denote this particle by $\mathbb{I} \in \mathbb{C}$. Also note that every particle a has an antiparticle $\bar{a}$ with conjugate charge and that $\mathbb{I} = \bar{\mathbb{I}}$.

Just as two spin-1/2 particles may combine to form a spin-1 or spin-0 particle so too can two particular anyons fuse into more than one particular anyon. The different possible fusions are known as *fusion channels.* So we have,

$$a \times b = \sum_{c \in \mathbb{C}} N_{ab}^c c \tag{2.27}$$

where $a \times b$ indicates a fused with b, N_{ab}^c is a non-negative integer indicating the number of ways charge a and charge b can be combined to form c, and $\mathbb{C}$ is the finite set of anyonic charges (sometimes referred to as *superselection sector* labels). It should be obvious that $N_{a\mathbb{I}}^c = \delta_{ac}$, and that $N_{ab}^{\mathbb{I}} = \delta_{b\bar{a}}$.

If, for a charge a,

$$\sum_c N_{ab}^c = \mathbb{I} \tag{2.28}$$

for every charge b, then a must correspond to abelian anyons. In order for the anyons to have a non-abelian representation of the braid group there must exist one pair of charges such that

$$\sum_c N_{ab}^c > \mathbb{I} \tag{2.29}$$

which is equivalent to saying that there must be a pair of charges a and b with multiple fusion channels.

Another way to distinguish abelian and non-abelian anyons is to examine their *quantum dimension*. For a charge a, its quantum dimension d_a is a measure of the amount of entropy added to the system by the presence of the charge. For an abelian charge we have $d_a = 1$, and for a non-abelian charge we have $d_a > 1$. Here we can define the total quantum dimension of an anyon model as

$$\mathcal{D} = \sqrt{\sum_a d_a^2}. \tag{2.30}$$

It is useful at this point to adopt a diagrammatic formalism to discuss anyon models. Again thinking of anyons as worldlines, with time increasing in the upward direction, where reversing the direction of the arrow is equivalent to charge conjugation.

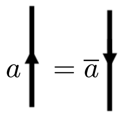

(2.31)

For each vector product there exists a fusion vector space V^c_{ab} (charges a & b combine to form charge c), and corresponding splitting space V^{ab}_c , where $dim(V^c_{ab}) = N^c_{ab}$. Defined as

$(d_c/d_a d_b)^{1/4}$

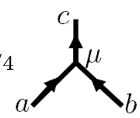

$= \langle a, b; c, \mu| \in V^c_{ab}$ (2.32)

$(d_c/d_a d_b)^{1/4}$

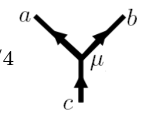

$= |a, b; c, \mu\rangle \in V^{ab}_c$ (2.33)

where $|a, b; c, \mu\rangle$ is some set of orthonormal basis vectors[4], with $\mu = 1, ..., N^c_{ab}$ and the factor $(d_c/d_a d_b)^{1/4}$, which is included to conform with the isotopy invariant convention discussed in [30]. Where Isotopy[5] is used to construct equivalence relations in *Knot* theory. Essentially telling us whether one knot may be continuously deformed into another. Our strands may be considered knots in this context as all open endpoints should be thought of as ending on some boundary through which isotopy is not permitted.

[4]The convention used throughout this paper that latin letters label particles and greek letters label vertices.

[5]Isotopy$\subset$Homotopy

The concept of inner product is conveyed diagrammatically as

$\langle a, b; c, \mu | a, b; c', \mu' \rangle = (d_c/d_a d_b)^{1/4}$ 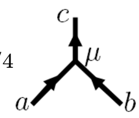 $.(d_c/d_a d_b)^{1/4}$ 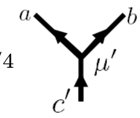 (2.34)

$\Rightarrow (d_c/d_a d_b)^{1/2}$ 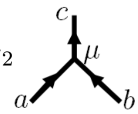 $\cdot$ 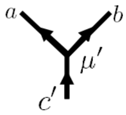 $= \delta_{c,c'}\delta_{\mu,\mu'}$ (2.35)

$\Rightarrow$ 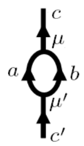 $= \delta_{cc'}\delta_{\mu\mu'}\sqrt{\frac{d_a d_b}{d_c}}$  (2.36)

which explicitly forbids *"tadpole"* diagrams and diagrammatically encodes charge conservation. An important special case of this is $c = 1$, where the equation reduces to

 $= d_a = d_{\overline{a}}$ (2.37)

showing that a charged, unknotted loop *evaluates* to its quantum dimension. When we say that we *evaluate* a particle or worldline, we mean that that we consider no further fusion or braiding in the life of the particle. This is represented by closing a line back in on itself.

The standard completeness relation $\sum\limits_i |i\rangle\langle i| = \mathbb{I}$, where $|i\rangle$ is the orthonormal basis is given, in our diagrammatic formalism, by

$|a, b; c, \mu\rangle\langle a, b; c, \mu| = (d_c/d_a d_b)^{1/4}$ 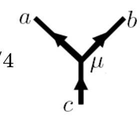 $.(d_c/d_a d_b)^{1/4}$ 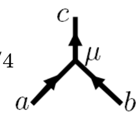 (2.38)

$\Rightarrow$ 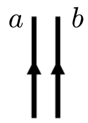 $= \sum\limits_{c,\mu}\sqrt{\frac{d_c}{d_a d_b}}$ 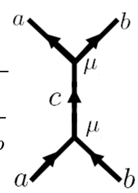 (2.39)

One last important relation is given by evaluating a and b

$\Rightarrow$ 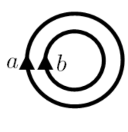 $(\equiv d_a d_b) = \sum\limits_{c,\mu}\sqrt{\frac{d_c}{d_a d_b}}$ 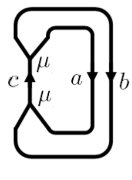 $= \sum\limits_c N_{ab}^c d_c$ (2.40)

These diagrammatic equations are also valid within larger more complicated diagrams, which will be essential later on. [3, 4, 30–32]

2.5 Some of the other methods required

What follows are very brief sections introducing the various other techniques, described in [3, 4], to the extent which we will need them later.

2.5.1 F-moves

F-moves are the set of unitary isomorphisms between different decompositions of the 4-anyon space V_d^{abc} into tensor products of two 3-anyon spaces (i.e. $\bigoplus_e V_e^{ab} \bigotimes V_d^{ec}$)[6] that are considered simply a change of basis.

They are related to each other by

$$[(F_d^{abc})^\dagger]_{(f,\mu,\nu)(e,\alpha,\beta)} = [F_d^{abc}]^*{}_{(e,\alpha,\beta)(f,\mu,\nu)} = [(F_d^{abc})^{-1}]_{(f,\mu,\nu)(e,\alpha,\beta)} \tag{2.41}$$

and are related to quantum numbers by

$$[F_d^{abc}]_{\mathbb{I}(c,\mu,\nu)} = [(F_d^{abc})^{-1}]_{(c,\mu,\nu)\mathbb{I}} = \sqrt{\frac{d_c}{d_a d_c}}\delta_{\mu\nu} \tag{2.42}$$

Two such useful F-move examples are

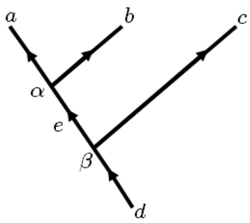

$$= \sum_{f,\mu,\nu} [F_d^{abc}]_{(e,\alpha,\beta)(f,\mu,\nu)} \tag{2.43}$$

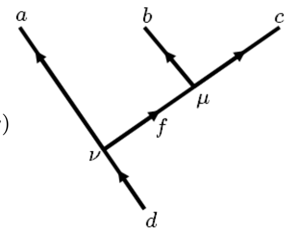

and

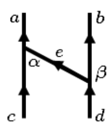

$$= \sum_{f,\mu,\nu} [F_{cd}^{ab}]_{(e,\alpha,\beta)(f,\mu,\nu)} \tag{2.44}$$

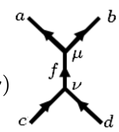

[6] $\bigoplus_e$ is the **direct sum**, which is used to combine several *modules* into a larger *module*. Here a vector space can be considered as a module over a field.

2.5.2 R-moves

The R-move R_{ab} is a unitary braiding operator of pairs of anyons equivalent to σ_i in section 2.3, but here $a \sim i$ and $b \sim (i+1)$. They are defined as

$$R_{ab}|a, b; c, \mu\rangle = \sum_v [R_c^{ab}]_{\mu\nu} |b, a; c, v\rangle \tag{2.45}$$

$\Rightarrow$ 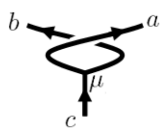 $= \sum_v [R_c^{ab}]_{\mu\nu}$ 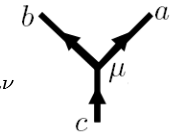 (2.46)

And are related to each other by

$$(R_{ab}R_{cd})^\dagger = (R_{ab}R_{cd})^{-1} = R_{dc}^{-1}R_{ba}^{-1} \tag{2.47}$$

These R-moves can be related to the topological spin, θ_a, of a particle a, through the equation

$$\sum_\lambda [R_c^{ab}]_{\mu\lambda}[R_c^{ba}]_{\lambda\nu} = \frac{\theta_c}{\theta_a\theta_b}\delta_{\mu\nu} \tag{2.48}$$

Where θ_a is related to the ordinary spin of a particle s_a by

$$\theta_a = e^{i2\pi s_a} \tag{2.49}$$

and is defined diagrammatically as

$\theta_a = \frac{1}{d_a}$ 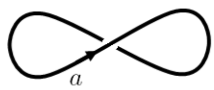 (2.50)

2.5.3 Topological S-matrix and the Monodromy Scalar

The Topological S-matrix S_{ab} is defined in terms of quantum dimension as

$S_{ab} = \frac{1}{\mathcal{D}}$  , $\qquad \mathcal{D} = \sqrt{\sum_a d_a^2} = \frac{1}{S_{\mathbb{I}\mathbb{I}}}$ (2.51)

And is described by the relations

$$S_{ab} = S_{ba} = \overline{(S^{-1})}_{ab} = \overline{S}_{\overline{a}b}, \qquad d_a = \frac{S_{\mathbb{I}a}}{S_{\mathbb{I}\mathbb{I}}} \tag{2.52}$$

It is important because of its relation to the Monodromy[7] scalar M_{ab},the value of which describes the statistics of a theory.

$$|M_{ab}| \begin{cases} = 1 & \text{abelian statistics} \\ < 1 & \text{non-abelian statistics} \end{cases} \tag{2.53}$$

In terms of the S-matrix M_{ab} is defined as

$M_{ab} = \frac{d_a}{d_b}$  $= \frac{S_{ab}S_{\mathbb{I}\mathbb{I}}}{S_{\mathbb{I}a}S_{\mathbb{I}b}}$ (2.54)

The S-matrix is also diagrammatically important as it allows us to remove closed loops from lines.

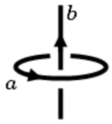 $= \frac{S_{ab}}{S_{\mathbb{I}b}}$  (2.55)

To see how the Monodromy scalars relate to each other consider first removing the loop e from the following diagram

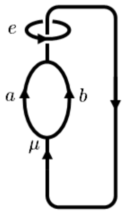 $= \frac{S_{ce}}{S_{\mathbb{I}c}}$ 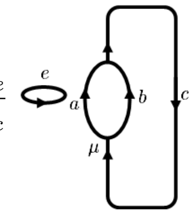 (2.56)

and then reconnecting it around the a strand

$\Rightarrow \quad =$ 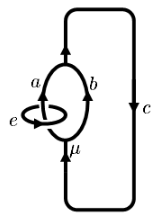 $\cdot \frac{S_{ce}}{S_{\mathbb{I}c}} \cdot \frac{S_{\mathbb{I}a}}{S_{ae}}$ (2.57)

which, looking at Eq.2.54, we see is equivalent to

$$\frac{M_{ce}}{M_{ae}} = \frac{S_{ce}S_{\mathbb{I}\mathbb{I}}}{S_{\mathbb{I}c}S_{\mathbb{I}e}} \cdot \frac{S_{\mathbb{I}a}S_{\mathbb{I}e}}{S_{ae}S_{\mathbb{I}\mathbb{I}}} = \frac{S_{ce}}{S_{\mathbb{I}c}} \cdot \frac{S_{\mathbb{I}a}}{S_{ae}} \tag{2.58}$$

but in our diagram e wrapping c is equivalent to e wrapping a and b, so we

[7] Monodromy is the study of how objects behave when moved around a singularity. In complex analysis it is related to the idea of a punctured disk, which is in turn related to topological concepts such as braiding.

could equally have said

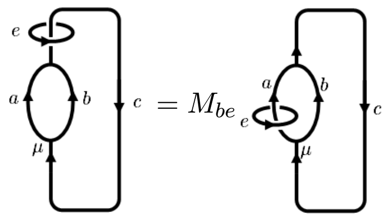

(2.59)

which leads to the important relation

$$M_{be} = \frac{M_{ce}}{M_{ae}} \tag{2.60}$$

[3,32]

2.5.4 Quantum Trace and Partial Quantum Trace

For a general system we use the notation

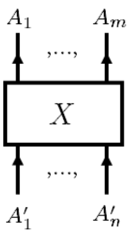

$$= X \in V^{A_1,\ldots,A_m}_{A'_1,\ldots,A'_n} = \sum_{\substack{a_1,\ldots,a_m \\ a'_1,\ldots,a'_n}} V^{a_1,\ldots,a_m}_{a'_1,\ldots,a'_n} \tag{2.61}$$

where X is a general operator acting on n input anyons and m output anyons. The capitalized anyons $A_1, ..., A_m$ & $A'_1, ..., A'_m$ indicate a direct sum over all possible charges. For the tensor product of an operator X, acting on anyons labelled by A and an operator Y on anyons labelled by B, we use the diagrammatic representation

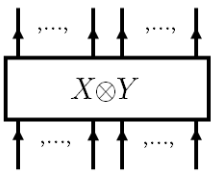

$=$

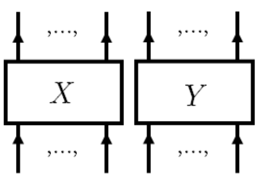

(2.62)

The quantum trace of the system X, $\widetilde{Tr}X$, is defined by matching the input line A_i to A'_i for all i.

$$\widetilde{Tr}X = \widetilde{Tr}$$
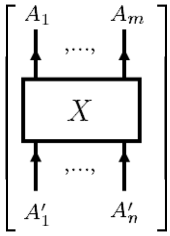

$$=$$
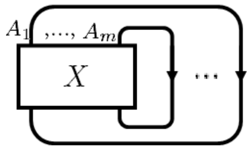

(2.63)

We cannot, however, connect lines of different anyonic charges, doing so would violate charge conservation and the resultant diagram would evaluate to 0.

The standard *Tr*ace and Quantum *Tr*ace are related to each other by

$$TrX = \sum_c \frac{1}{d_c}\widetilde{Tr}X_c, \qquad \widetilde{Tr}X = \sum_c d_c TrX_c \tag{2.64}$$

$$X = \sum_c X_c, \qquad X_c \in V_c^{A_1,\ldots,A_n} \otimes V^c_{A'_1,\ldots,A'_n} \tag{2.65}$$

The Partial Quantum Trace, $\widetilde{Tr_B}X$, over an anyon B, can only be taken if B is one of the outer anyons (i.e. at position A_1 or A_m above) due to the fact that B can't be treated as independent while still *in the midst* of the remaining anyons. For an operator $X \in V^{A_1,\ldots,A_n,B}_{A'_1,\ldots,A'_n,B'}$ or $X \in V^{B,A_1,\ldots,A_n}_{B',A'_1,\ldots,A'_n}$, the partial trace is defined by joining only B & B' as either

$$\widetilde{Tr}_B X =$$
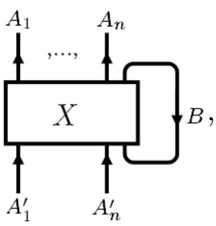

OR
$$\widetilde{Tr}_B X =$$
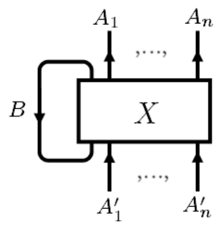

(2.66)

It is also true that B need not be just a single anyon in our system, but may we be a subsystem of anyons $B = (B_1, ..., B_m)$. However, provided B is contiguous we may treat it as a single anyon. Where $\widetilde{Tr}_B \equiv \widetilde{Tr}_{B_m}, ..., \widetilde{Tr}_{B_1}$ and we simply iterate the the operation starting at the edge as

$$\widetilde{Tr}_B \equiv \widetilde{Tr}_{B_m}, ..., \widetilde{Tr}_{B_1} =$$
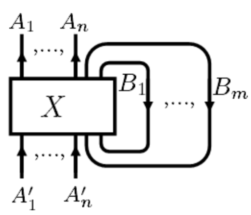

(2.67)

and similarly for B at the other edge.

By way of demonstration we apply the Partial Quantum Trace to one of the equations we looked at in Section 2.4

$\widetilde{Tr}_B$ 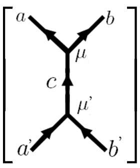

$=$ 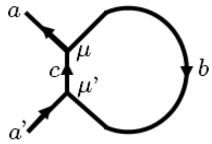

(2.68)

which, using Eq 2.44, leads to

$$= \sum_{e,\alpha,\beta} [(F^{ab}_{a'b'})^{-1}]_{(c,\mu\mu')(e,\alpha,\beta)} \tag{2.69}$$
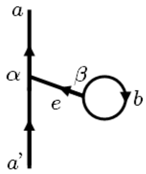

For charge conservation we must have $a = a'$ and $b = b'$ which leads to

$$= [(F^{ab}_{ab})]_{(c,\mu,\mu')\mathbb{I}} \tag{2.70}$$
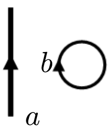

$$= \sqrt{\frac{d_c}{d_a d_b}} \delta_{\mu,\mu'} \tag{2.71}$$
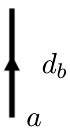

$\Rightarrow \quad \widetilde{Tr}_B$ 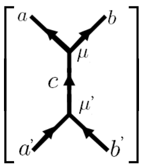

$= \sqrt{\frac{d_c d_b}{d_a}} \delta_{\mu,\mu'}$ 

(2.72)

$\widetilde{Tr}$ gives us one more important relation for the S-matrix

$$S_{ab} = \mathcal{D}^{-1} \widetilde{Tr}[R_{ba} R_{ab}] = \frac{1}{\mathcal{D}} \tag{2.73}$$


2.5.5 States and Density Matrices

To properly describe the state $|\psi\rangle$ of a system of anyons one must start with the creation from vacuum of a particle/anti-particle pair with respective charges c and $\overline{c}$

$$|\psi\rangle = \sum_c \psi_c |c, \overline{c}; \mathbb{I}\rangle = \frac{1}{(d_c)^{1/2}} \tag{2.74}$$
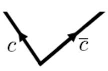

It then is necessary to specify all the splitting channels starting from the vacuum. So for the particular case where c splits into just a and b (or equally $\overline{c}$

splits into $\overline{a}$ and $\overline{b}$) we have the state

$$|\psi\rangle = \sum_{a,b,c,\mu} \psi_{a,b,c,\mu} |a, b; c, \mu\rangle |c, \overline{c}; \mathbb{I}\rangle \tag{2.75}$$

$$= \sum_{a,b,c,\mu} \frac{\psi_{a,b,c,\mu}}{(d_a d_b d_c)^{1/4}} \tag{2.76}$$

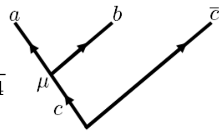

We note that the total charge of the system is zero as desired.

Using this approach allows us to exactly specify the state and to conserve charge. However, this approach, for systems with many more splitting channels, becomes difficult to deal with. It also makes it very difficult to evaluate just a subsystem. For these reasons we will instead use the density matrix approach outlined below.

For an arbitrary two anyon system, the density matrix

$$\rho := \sum_{\substack{a,a',b,b' \\ c,\mu,\mu'}} \rho_{(a,b,c,\mu)(a',b',c,\mu')} \frac{1}{d_c} |a, b; c, \mu\rangle \langle a', b'; c, \mu'| \tag{2.77}$$

using Eq.2.38, with a',b',μ' replacing the input set of a,b,μ, (note that c is unaffected due to charge conservation) this reduces to

$$\rho = \sum_{\substack{a,a',b,b' \\ c,\mu,\mu'}} \frac{\rho_{(a,b,c,\mu)(a',b',c,\mu')}}{(d_a d_b d_{a'} d_{b'} d_c^2)^{1/4}} \tag{2.78}$$

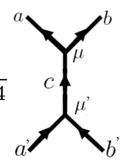

A normalisation is chosen such that

$$\widetilde{Tr}[\rho] = \sum_{a,b,c,\mu} \rho_{(a,b,c,\mu)(a,b,c,\mu)} = 1 \tag{2.79}$$

The main use of the density matrix approach is that it allows us to a evaluate a subsystem. Consider another density matrix ρ' defined as

$$\rho' = \sum_{\substack{a,a',b,b' \\ c,c',\mu,\mu'}} \rho_{(a,b,c,\mu)(a',b',c',\mu')} |a, b; c, \mu\rangle |c, \overline{c}; \mathbb{I}\rangle \langle c', \overline{c'}; \mathbb{I}| \langle a', b'; c, \mu'| \tag{2.80}$$

$$= \sum_{\substack{a,a',b,b'\\c,c',\mu,\mu'}} \frac{\rho_{(a,b,c,\mu)(a',b',c',\mu')}}{(d_a d_b d_c d_{a'} d_{b'} d_{c'})^{1/4}} \tag{2.81}$$

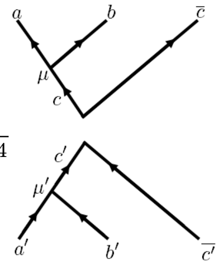

Then by taking the partial trace over $\overline{c}$ we see

$$\widetilde{Tr}_{\overline{c}}[\rho'] = \sum_{\substack{a,a',b,b'\\c,c',\mu,\mu'}} \frac{\rho_{(a,b,c,\mu)(a',b',c',\mu')}}{(d_a d_b d_c d_{a'} d_{b'} d_{c'})^{1/4}} \tag{2.82}$$

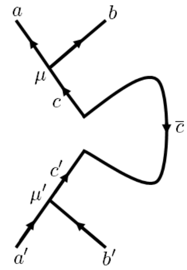

then, by charge conservation we must let $c = c'$, which leads us to

$$\widetilde{Tr}_{\overline{c}}[\rho'] = \sum_{\substack{a,a',b,b'\\c,\mu,\mu'}} \frac{\rho_{(a,b,c,\mu)(a',b',c,\mu')}}{(d_a d_b d_{a'} d_{b'} d_c^2)^{1/4}} \tag{2.83}$$

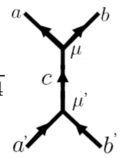

which is exactly ρ. So we have the relation

$$\rho = \widetilde{Tr}_{\overline{c}}[\rho'] \tag{2.84}$$

which allows us to easily consider a subsystem.

3 Topological Quantum Computing Via Interferometry

In this section we see that interferometry not only offers a us a way to analyze the statistics of anyons, but also to implement a NOT-gate [5].

We will begin by looking at the Mach-Zehnder type interferometer as a test case, then expand the work done in [3] studying the 2-point Fabry-Pérot interferometer to encompass the 3-point interferometer [5].

3.1 Mach-Zehnder Interferometer as a Test case

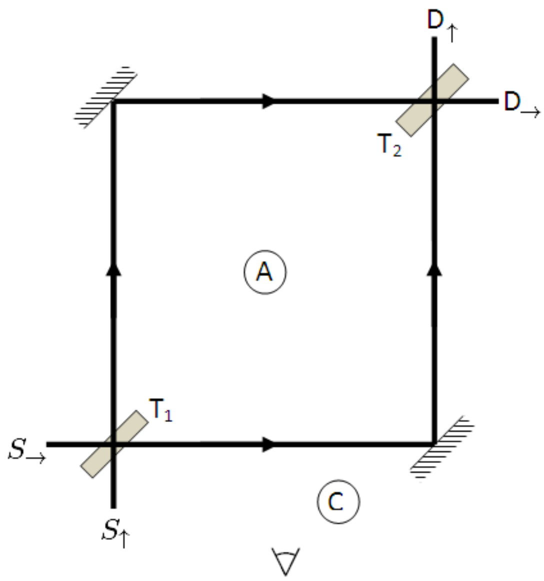

In this section we consider an idealized Mach-Zehnder interferometer [33, 34] for quasi-particles with non-Abelian braiding statistics, which supports an arbitrary anyon model.

Figure 3.1: **Mach-Zehnder Interferometer** - A: Target anyons, B: Probe anyons, C: Entangled anyons located outside the central interferometry, T_1,T_2: Beam-splitters, D: Detectors, $\lhd$: Position we are *viewing* from when considering braiding operations. This is arbitrary but important to define

We note that within a FQH system there exist what are referred to as intended quasiparticles and unintended quasiparticles. The intended quasiparticles are those that we have created (and whose positions we know) to perform our quantum computation. The unintended quasiparticles are those which have been introduced to the system without our knowledge. An example of this is the creation via thermal fluctuations of quasiparticle-quasihole pairs which may encircle an intended quasiparticle before annihilating [though for an error to be introduced the unintended pair must encircle two intended quasiparticles. So, to minimize thermal fluctuations and hence exponentially suppress errors, TQ computations must be performed at temperatures far below the energy level for quasiparticle-quasihole pair creation. For our calculations we will ignore such errors and only concern ourselves with intended quasiparticles.

We begin by positing the experimental ability (without concern for physical implementations) to

- Produce, isolate and position the desired anyons.
- Provide a manner of propulsion to produce a beam of probe anyons.
- Construct lossless beam-splitters and mirrors.
- Detect the probe anyons at the output.

We will consider A, B, C not to be a single anyon but instead to be a composites $A = (A_1...A_n)$, $B = (B_1...B_n)$, $C = (C_1...C_n)$, in charge superposition. We also wish that A and C be entangled only with each other.

A probe anyon B is sent into the system at input $S_\rightarrow$ or $S_\rightarrow$. We use the subscript B_s where $s = (\rightarrow, \uparrow)$ to denote the choice. This corresponds to the two component vector notation

$$\begin{pmatrix} 1 \\ 0 \end{pmatrix} = |\rightarrow\rangle, \qquad \begin{pmatrix} 0 \\ 1 \end{pmatrix} = |\uparrow\rangle \tag{3.1}$$

which is necessary to keep track of the path the anyon follows through the interferometer.

The probe anyon B can either travel along the path over A acquiring a phase $e^{i\theta_2}$ (due to the Aharonov-Bohm effect [35, 36]) and the braid R^{-1}_{AB}, or along the path between A and C picking up a phase $e^{i\theta_1}$ and R_{BA}.

The mirrors and beam-splitters have transmission and reflection the coefficients

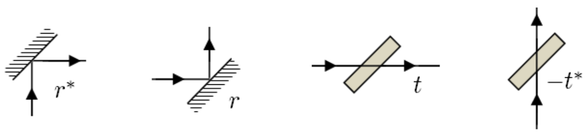

(3.2)

and are represented by the matrix

$$T_j = \begin{bmatrix} t_j & r_j^* \\ r_j & -t_j^* \end{bmatrix}, \qquad |t_j|^2 + |r_j|^2 = 1 \tag{3.3}$$

The density matrix of the target system A is

$$\rho^A = \sum_{\substack{a,a',b,b' \\ c,\mu,\mu'}} \frac{1}{d_c} \rho^A_{(a,c;f,\mu)(a',c';f,\mu')} |a,c;f,\mu\rangle\langle a',c';f,\mu'| \tag{3.4}$$

$$= \sum_{all} \frac{\rho^A_{(a,c;f,\mu)(a',c';f,\mu')}}{(d_a d_{a'} d_c d_{c'} (d_f)^2)^{1/4}} \tag{3.5}$$

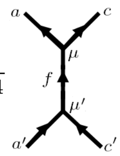

where $\rho^A_{(a,c;f,\mu)(a',c';f,\mu')}$ is a specific coefficient and $\sum_{all}$ merely indicates that we are summing over the same indices again. The density matrix of the probe system B is given by

$$\rho^B = \sum_{\substack{d,d',b_s,b'_s \\ h,\lambda,\lambda'}} \frac{1}{d_h} \rho^B_{(d,b_s;h,\lambda)(d',b'_s;h,\lambda')} |d,b;h,\lambda\rangle\langle d',b'_s;h,\lambda'| \tag{3.6}$$

$$= \sum_{all} \frac{\rho^B_{(d,b_s;h,\lambda)(d',b'_s;h,\lambda')}}{(d_d d_{d'} d_{b_s} d_{b'_s} (d_h)^2)^{1/4}} \tag{3.7}$$

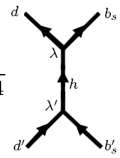

where s indicates the incident direction of the specific anyon b. B's entangled partner D is considered to have been sent off far to the left outside the diagram.

The unitary operator representing the probe anyons passing through the interferometer is

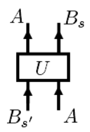

$$= \underbrace{e^{i\theta_1} \begin{bmatrix} t_1 r_2^* & r_1^* r_1^* \\ -t_1 t_2^* & -r_1^* t_2^* \end{bmatrix}_{s,s'} R_{BA}}_{W} + \underbrace{e^{i\theta_2} \begin{bmatrix} r_1 t_2 & -t_1^* t_2 \\ r_1 r_2 & -t_1^* r_2 \end{bmatrix}_{s,s'} R_{BA}^{-1}}_{X} \tag{3.8}$$

and its hermitian conjugate is

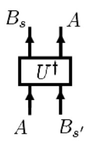

$$= \underbrace{e^{-i\theta_1} \begin{bmatrix} t_1^* r_2 & -t_1^* t_2 \\ r_1 r_2 & -r_1 t_2 \end{bmatrix}_{s,s'} R_{AB}^{-1}}_{Y} + \underbrace{e^{-i\theta_2} \begin{bmatrix} r_1^* t_2^* & r_1^* r_2^* \\ -t_1 t_2^* & -t_1 r_2^* \end{bmatrix}_{s,s'} R_{AB}}_{Z} \tag{3.9}$$

where

$$U = T_2 \Sigma T_1, \qquad \Sigma = \begin{bmatrix} 0 & e^{i\theta_2} R_{AB}^{-1} \\ e^{i\theta_1} R_{BA} & 0 \end{bmatrix} \tag{3.10}$$

We choose at this point to label the individual components to make more apparent a calculation later on.

The braiding of C with the probe is given by

$$V = \begin{bmatrix} R_{CB}^{-1} & 0 \\ 0 & R_{CB}^{-1} \end{bmatrix} = \tag{3.11}$$

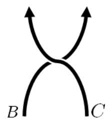

Once B is measured at one of the detectors, we remove it and its entangled partner from the system. Diagrammatically we trace anyons B and D out of the system, so that the overall state of the system is

$$\rho = VU(\rho^B \otimes \rho^A)U^\dagger V^\dagger \tag{3.12}$$

and we apply the orthogonal measurement collapse projection, with $\Pi_s = |s\rangle\langle s|$, such that

$$\rho \mapsto \frac{\Pi_s \rho \Pi_s}{Pr(s)}, \qquad Pr(s) = \widetilde{Tr}[\rho \Pi_s] \tag{3.13}$$

3.1.1 Single Probe

For simplicity we will consider a single probe anyon b, with density matrix $\rho^b = |\overline{b}, b_\uparrow; \mathbb{I}\rangle\langle\overline{b}, b_\uparrow; \mathbb{I}|$. Since the $s = \rightarrow$ case is looked at in [3] we will look at the $s = \uparrow$ case. So for a single probe anyon, Eqs. 3.12, 3.13 correspond to
The tracing out of $\overline{b}$ and b_s, and the fusion/splitting vertices labels μ', μ, are not illustrated in this diagram for clarity's sake. The partial traces would simply result in the $\overline{b}$ being looped back around to itself on the left side of the diagram, and for b_s being looped back around on itself on the right side of the diagram. Both without any further interaction of course.

$$\rho = VU(\rho^b \otimes \rho^A)U^\dagger V^\dagger \tag{3.14}$$

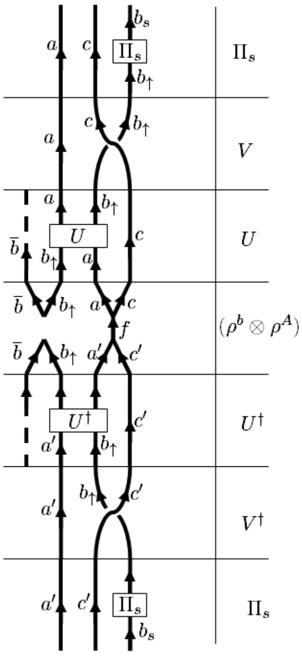

Figure 3.2: Diagrammatic interpretation of the equation 3.14

By inverting Eq.2.44 we get

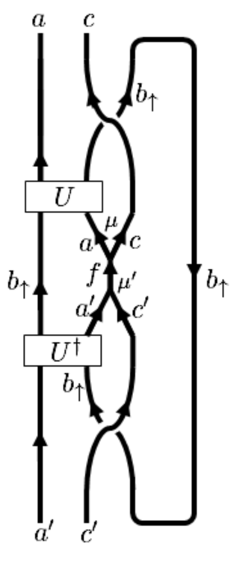

$$= \sum_{e,\alpha,\beta} [(F^{ac}_{a'c'})^{-1}]_{(f,\mu,\mu')(e,\alpha,\beta)} \tag{3.15}$$

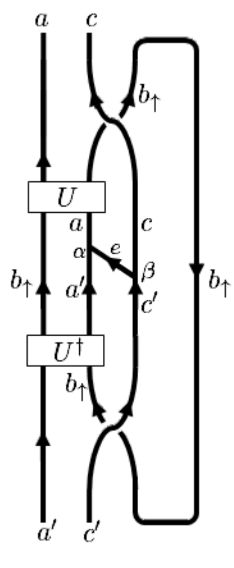

Now we look at the four cases from U and $U^\dagger$, where W,X,Y, and Z are defined in Eqs. 3.8, 3.9, 1.

$$\begin{pmatrix}0 & 1\end{pmatrix}^{\uparrow} W \begin{pmatrix}1\\0\end{pmatrix}^{\rightarrow} \times \begin{pmatrix}1 & 0\end{pmatrix}^{\uparrow} Y \begin{pmatrix}0\\1\end{pmatrix}^{\rightarrow} = |t_1|^2|t_2|^2 \tag{3.16}$$

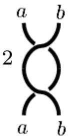

2.

$$\begin{pmatrix}0 & 1\end{pmatrix}^{\uparrow} X \begin{pmatrix}1\\0\end{pmatrix}^{\rightarrow} \times \begin{pmatrix}1 & 0\end{pmatrix}^{\uparrow} Z \begin{pmatrix}0\\1\end{pmatrix}^{\rightarrow} = |r_1|^2|r_2|^2 \tag{3.17}$$

3.

$$\begin{pmatrix}0 & 1\end{pmatrix}^{\uparrow} W \begin{pmatrix}1\\0\end{pmatrix}^{\rightarrow} \times \begin{pmatrix}1 & 0\end{pmatrix}^{\uparrow} Z \begin{pmatrix}0\\1\end{pmatrix}^{\rightarrow} = -t_1 r_2^* r_1^* t_2^* e^{i(\theta_1-\theta_2)} \tag{3.18}$$

4.

$$\begin{pmatrix}0 & 1\end{pmatrix}^{\uparrow} X \begin{pmatrix}1\\0\end{pmatrix}^{\rightarrow} \times \begin{pmatrix}1 & 0\end{pmatrix}^{\uparrow} Y \begin{pmatrix}0\\1\end{pmatrix}^{\rightarrow} = -t_1^* r_2 r_1 t_2 e^{-i(\theta_1-\theta_2)} \tag{3.19}$$

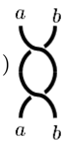

which gives us

$$= \sum_{e,\alpha,\beta} [(F^{ac}_{a'c'})^{-1}]_{(f,\mu,\mu')(e,\alpha,\beta)}$$

$$\times \Bigg\{ |t_1|^2|t_2|^2$$

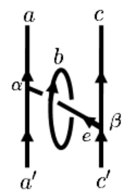

$$- t_1 r_2^* r_1^* t_2^* e^{i(\theta_1-\theta_2)}$$

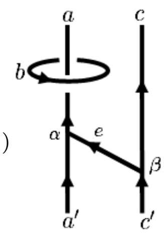

$$+ |r_1|^2|r_2|^2$$

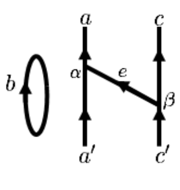

$$- t_1^* r_2 r_1 t_2 e^{-i(\theta_1-\theta_2)}$$

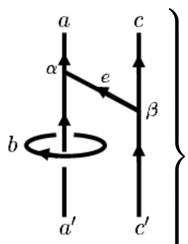

$$\Bigg\} \tag{3.20}$$

The exact forms of the four braid diagrams may not be obvious initially. To see how we arrive at them, replace the U and $U^\dagger$ (keeping α,e and β intact) of

Eq. 3.15, with the braids of Eqs. 3.16-19. Then imagine the worldlines as strings (or use actual strings), and deform them, bearing in mind that we consider a, a', c, c' to end on some surface through which deformations are not allowed.

We then use Eq. 2.37, Eq. 2.44 and Eq. 2.55 to get

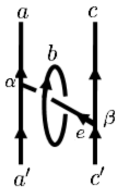

$$= M_{eb}[F^{ac}_{a'c'}]_{(e,\alpha,\beta)(f',\nu,\nu')}d_b \tag{3.21}$$

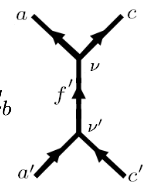

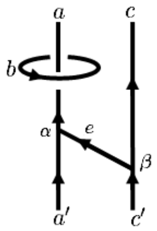

$$= M_{ab}[F^{ac}_{a'c'}]_{(e,\alpha,\beta)(f',\nu,\nu')}d_b \tag{3.22}$$

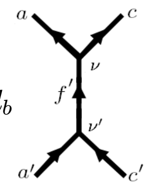

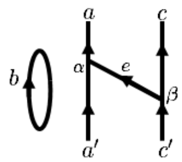

$$= [F^{ac}_{a'c'}]_{(e,\alpha,\beta)(f',\nu,\nu')}d_b \tag{3.23}$$

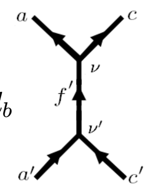

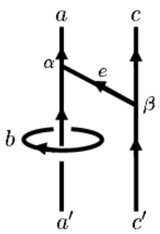

$$= M^*_{a'b}[F^{ac}_{a'c'}]_{(e,\alpha,\beta)(f',\nu,\nu')}d_b \tag{3.24}$$

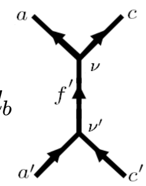

where M^* indicates the clockwise rotation of b around a' (since reversing the direction of an arrow is akin to conjugation).

This leads to our result

$$= d_b \sum_{\substack{e,\alpha,\beta \\ f',\nu,\nu'}} [(F^{ac}_{a'c'})^{-1}]_{(f,\mu,\mu')(e,\alpha,\beta)}[F^{ac}_{a'c'}]_{(e,\alpha,\beta)(f',\nu,\nu')}p^{\uparrow}_{aa'e,b} \tag{3.25}$$

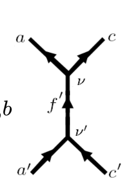

with

$$\begin{aligned} p^{\uparrow}_{aa'e,b} = \quad & |t_1|^2|t_2|^2 M_{eb} - t_1 r_2^* r_1^* t_2^* e^{i(\theta_1-\theta_2)} M_{ab} \\ & +|r_1|^2|r_2|^2 - t_1^* r_2 r_1 t_2 e^{-i(\theta_1-\theta_2)} M^*_{a'b} \end{aligned} \tag{3.26}$$

For $s = \rightarrow$ the result given in [3] is

$$p^{\rightarrow}_{aa'e,b} = \begin{array}{l} |t_1|^2|r_2|^2 M_{eb} + t_1 r_2^* r_1^* t_2^* e^{i(\theta_1-\theta_2)} M_{ab} \\ +|r_1|^2|t_2|^2 + t_1^* r_2 r_1 t_2 e^{-i(\theta_1-\theta_2)} M^*_{a'b} \end{array} \tag{3.27}$$

For some general outcome s, the reduced density matrix of the target anyons is given by

$$\begin{aligned} \rho^A &= \tfrac{1}{Pr(s)} \widetilde{Tr}_{\overline{B},B}[\Pi_s \rho \Pi_s] \\ &= \sum_{\substack{a,a',c,c',f,\mu,\mu' \\ e,\alpha,\beta,f',\nu,\nu'}} \frac{\rho^A_{(a,c;f,\mu)(a',c';f,\mu')}}{(d_a d_{a'} d_c d_{c'} d_f^2)^{1/4}} \frac{p^s_{aa'e,b}}{Pr(s)} \\ &\times [(F^{ac}_{a'c'})^{-1}]_{(f,\mu,\mu')(e,\alpha,\beta)} [F^{ac}_{a'c'}]_{(e,\alpha,\beta)(f',\nu,\nu')} p^s_{aa'e,b} \end{aligned} \tag{3.28}$$

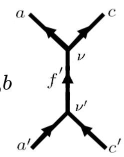

$$\begin{aligned} &= \sum_{all} \frac{\rho^A_{(a,c;f,\mu)(a',c';f,\mu')}}{(d_f d_{f'})^{1/2}} \frac{p^s_{aa'e,b}}{Pr(s)} [(F^{ac}_{a'c'})^{-1}]_{(f,\mu,\mu')(e,\alpha,\beta)} \\ &\times [F^{ac}_{a'c'}]_{(e,\alpha,\beta)(f',\nu,\nu')} \; |a,c;f',\nu\rangle\langle a',c';f',\nu'| \end{aligned} \tag{3.29}$$

To find the probability of measurement outcome s we now take the quantum trace of the target system, which projects on $e = 1$, giving

$$Pr(s) = \widetilde{Tr}[\rho \Pi_s] = \sum_{a,c,f,\mu} \rho^A(a,c;f,\mu)(a,c;f,\mu) p^s_{aa1,b} \tag{3.30}$$

We note that we have a well defined probability distribution since

$$\begin{aligned} p^{\uparrow}_{aa1,b} &= |t_1|^2|t_2|^2 + |r_1|^2|r_2|^2 - 2Re\left(t_1 t_2^* r_1^* r_2^* e^{i(\theta_1-\theta_2)} M_{ab}\right) \\ p^{\rightarrow}_{aa1,b} &= |t_1|^2|r_2|^2 + |r_1|^2|t_2|^2 + 2Re\left(t_1 r_2^* r_1^* t_2^* e^{i(\theta_1-\theta_2)} M_{ab}\right) \end{aligned} \tag{3.31}$$

gives us

$$0 \leq p^s_{aa1,b} \leq 1, \qquad p^{\rightarrow}_{aa1,b} + p^{\uparrow}_{aa1,b} = 1 \tag{3.32}$$

For the general density matrix ρ^B we obtain a result by replacing $p^s_a a'e, b$ with

$$p^s_a a'e, B = \sum_b Pr_B(b) p^s_a a'e, b \tag{3.33}$$

where we define

$$Pr_B(b) = \sum_{d,h,\lambda} \rho^B_{(d,b_\rightarrow;h,\lambda)(d,b_\rightarrow;h,\lambda)} \tag{3.34}$$

3.2 Fabry-Pérot Interferometer as a NOT-gate

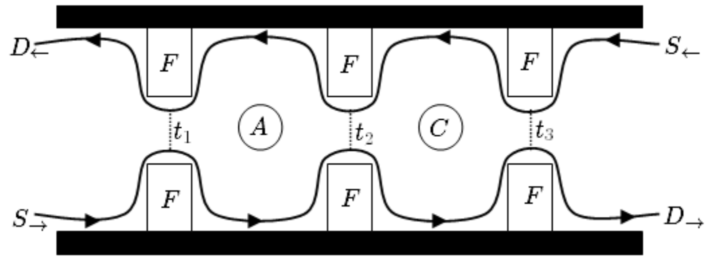

Figure 3.3: 3-Point contact Fabry-Pérot Interferometer [5, 37].

We will discuss in this section a the 3-Point Fabry-Pérot[1] type Interferometer of Fig.3.3. First focusing on the means by which it may be used to implement a NOT-gate, as outlined in [5], and then performing some calculations with the 2- and 3-point versions.

The Fabry-Pérot Interferometer consists of: a quantum Hall bar with two individually gated anti-dots, A and C, (*"humps"* in the potential) in the interior. Tunnelling is enabled at t_1, t_2, t_3, by applying a voltage to opposing F-gates which creates an anti-dot (not shown) between the gates. The arrowed line represents the path the electrons (which are confined to the edge of the sample by the FQHE) take when a current is applied. The region encompassed by the arrowed-lines contains an incompressible FQH liquid. Again, S and D represent the sources and detectors respectively.

To show how this may be used as a NOT-gate, we wish to

1. Initialize the qubit and measure its state:
   This is done by placing a charge $\frac{e}{2}$ on anti-dot A, which will be either occupied or unoccupied but *not* a superposition of the two. To determine the state we apply a voltage across the front and back gates so that tunnelling can occur with amplitudes t_1 and t_3. The longitudinal conductivity, σ_{xx}, is the probability that current entering from $S_\rightarrow$ will exit from $D_\leftarrow$. This is given (to lowest order) by the interference from the process of the current tunneling at t_1, and the process that the current travels right to tunnel

[1] There is much debate over the correct spelling of Pérot's name. In his own scientific publications he spelled his name with the accent, we choose here to respect his wishes. See http://www.sabix.org/documents/perot.pdf "Pérot ou Perot?".

at t_3. Where the state of the qubit, which is formed by the correlation between anti-dots A and C, is determined by the relative phases of the processes

$$\begin{aligned} |0\rangle &:= \sigma_{xx} \propto |t_1 + it_2|^2 \\ |1\rangle &:= \sigma_{xx} \propto |t_1 - it_2|^2 \end{aligned} \tag{3.35}$$

2. Flip the qubit:
   With initial state $|0\rangle$ (the choice of initial state $|0\rangle$ or $|1\rangle$ is arbitrary) we apply a voltage to the anti-dots so that a charge $\frac{e}{4}$ is transferred from A to C, so that each anti-dot now has a charge $\frac{e}{4}$. Note that the state is unaffected by this process. A voltage is now applied to the central gates so that *a single* quasiparticle of charge $\frac{e}{4}$ tunnels across t_2. To ensure that only one quasiparticle tunnels we can place, before the outset, a finely tuned anti-dot E between the central gates. By applying the voltage in stages, first to the bottom so that the anti-dot is filled by a charge $\frac{e}{4}$ quasiparticle, then turning off the current at the bottom and applying it to the top so the quasiparticle trapped at E tunnels across. E should be turned off at the beginning and end of the bit-flip process so that there are no quasiparticles there which could become entangled with our system.

   If the $\nu = \frac{5}{2}$ plateau is in the phase of the Moore-Read Pfaffian state, this will transform $|0\rangle$ to $|1\rangle$. However, if do not observe this state then we can conclude that our state is abelian.

3. Measure the new state:
   As with our initial measurement we allow tunnelling at t_1 and t_3, where we expect to find

$$\sigma_{xx} \propto |t_1 - it_2|^2 \longrightarrow |1\rangle \tag{3.36}$$

We now ask with what probability can this be performed, ie. what is the error rate, Γ, of this NOT-gate. A Bit-flip error will occur when an uncontrolled charge $\frac{e}{4}$ quasiparticle encircles one of the anti-dots by jumping across the Hall bar between A and C (essentially how we perform the Bit-flip but without our knowledge). A phase flip error will occur when an uncontrolled charge $\frac{e}{4}$ quasiparticle encircles both A and C. The rate for these processes is related to the longitudinal resistivity, from which we can put an upper bound on the error rate.

$$\frac{\Gamma}{\Delta} \sim \frac{T}{\Delta} e^{-\Delta/2T} \tag{3.37}$$

With values for the quasiparticle excitation gap $\Delta \approx 500$mK and lowest achieved measurement temperature $T \sim 5\text{mK}$ [5,6] we get

$$\frac{T}{\Delta}e^{-\Delta/2T} < 10^{-15} \tag{3.38}$$

which is incredibly low. However, this is a simplification and calculating the actual error rate for this system would need to consider multiple energy gaps, and the density and mobility of excited quasiparticles. Even so, these error rates are considerably lower than implementations in any other proposed architectures of quantum computation, where the estimated error is $\sim 10^{-4}$ [38].

3.2.1 2-point Gate Calculations

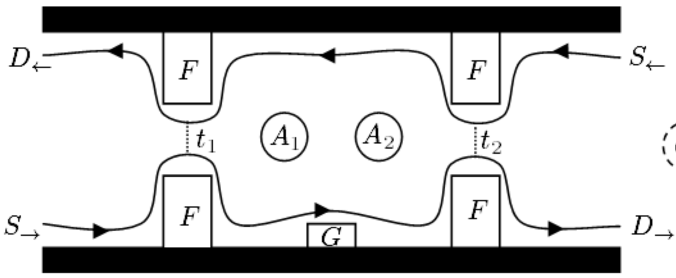

Figure 3.4: 2-Point contact Fabry-Perot Interferometer [3]. Where the gate G is used, experimentally, to change the shape and length of one of the paths. Two antidots are used to allow for the combined target to maintain a coherent superposition of anyonic charges. [39]

Before we look at the 3-point gate calculations, we will look at the slightly simpler 2-point case, constructing the unitary matrix describing the interactions and the density matrix of the system.

The set-up is as follows. We consider the source $S_\leftarrow$ and the detector (drain) $D_\rightarrow$ to be further right than the anyon C. Counter-clockwise motion over A results in $e^{i\theta_1}$ and counter-clockwise motion under A results in an acquired phase $e^{i\theta_2}$.

The tunneling and transmission coefficients are defined as

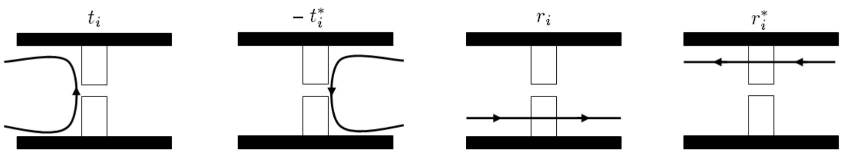

(3.39)

where we have simplified the diagrams, for clarity, by representing r_i as a straight line through the gate whereas in fact they must travel up over the gate and then back down as in Fig 3.4.

We work in the convention where moving along the top edge is defined by $\langle\leftarrow|$ and moving along the bottom edge is defined by $|\rightarrow\rangle$. Where

$$\begin{pmatrix}1\\0\end{pmatrix} = |\leftarrow\rangle, \qquad \begin{pmatrix}0\\1\end{pmatrix} = |\rightarrow\rangle \tag{3.40}$$

As before, to build up our Unitary matrix U we look at the components individually.

$U_{1,1}$: corresponding to $(\leftarrow,\leftarrow)$ which is an anyon B entering from $S_\leftarrow$ and exiting from $D_\leftarrow$.

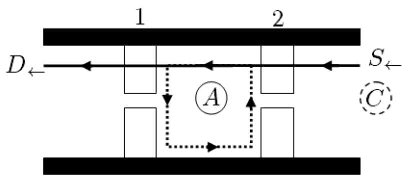

Ignoring the dotted line for a moment we see that the probe anyon B must undergo the braiding $R_{AB}R_{CB}$, acquire the phase $e^{i\theta}$, and also pick up the transmission coefficients $r_1^* r_2^*$. So we would have

$$U_{1,1} = r_1^* r_2^* e^{i\theta_2} R_{AB} R_{CB} \tag{3.41}$$

However, we must also consider the fact that B may be reflected at Gate 1 ($t_1^* R_{BA}$), travel under A ($e^{i\theta_2}$), be reflected back at Gate 2 ($t_2 R_{AB}$) and travel over A again ($e^{i\theta_1}$), which is represented by the dotted line. Furthermore it may do so indefinitely. To deal with this we introduce the *Wrapping* term

$$W_{AB} := \sum_{n=0}^{\infty} \left(-t_1^* t_2 e^{i(\theta_1+\theta_2)} R_{BA} R_{AB}\right)^n \tag{3.42}$$

where n is the number of times B encircles A. We should also note the mathematical relation

$$\sum_{n=0}^{\infty} (-A)^n = \frac{1}{1+A} \tag{3.43}$$

which allows us to write

$$W_{AB} = \frac{1}{\left(1 + t_1^* t_2 e^{i(\theta_1+\theta_2)} R_{BA} R_{AB}\right)} \tag{3.44}$$

So our actual component value is

$$U_{1,1} = r_1^* r_2^* e^{i\theta_1} R_{AB} W_{AB} R_{CB} \tag{3.45}$$

$U_{2,2}$: corresponding to $(\rightarrow, \rightarrow)$ which is an anyon B entering from $S_\rightarrow$ and exiting from $D_\rightarrow$.

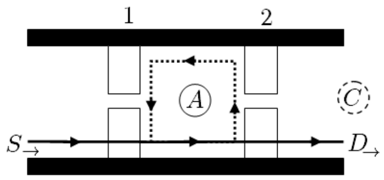

In a similar fashion to $U_{1,1}$ we can find our value to be

$$U_{2,2} = r_1 r_2 e^{i\theta_2} R_{BC} R_{BA} W_{BA} \tag{3.46}$$

$U_{1,2}$: corresponding to $(\rightarrow, \leftarrow)$ which is anyon B entering from $S_\rightarrow$ and exiting from $D_\leftarrow$. Slightly more complicated than the previous components of U, we have two separate paths. For $n = 0$ we have the case where only the

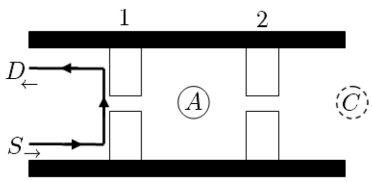

reflection coefficient t_1 is acquired. For the case $n \rightarrow \infty$ we must use our

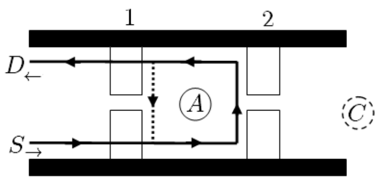

W term, which gives us

$$U_{1,2} = \frac{1}{t_1^*}(1 - |r_1|^2 W_{BA}) \tag{3.47}$$

The placement of W_{BA} may not be obvious, to make it so we expand out for $n = 1$, recalling the fact that $|t_j|^2 + |r_j|^2 = 1$, so we can write t_1 as

$\frac{1-|r_1|^2}{t_1^*}$, so we have

$$\begin{aligned} U_{1,2}^{(n=1)} &= \tfrac{1}{t_1^*}\left(1-|r_1|^2(1-t_1^*t_2e^{i(\theta_1+\theta_2)}R_{AB}R_{BA})\right) \\ &= t_1+|r_1|^2t_2e^{i(\theta_1+\theta_2)}R_{AB}R_{BA} \end{aligned} \tag{3.48}$$

which covers both our cases.

$U_{2,1}$: corresponding to $(\leftarrow,\rightarrow)$ which is anyon B entering from $S_\leftarrow$ and exiting from $D_\rightarrow$. Using the same method as $U_{1,2}$ we get

$$U_{2,1}=R_{BC}\frac{1}{t_2}(-1+|r_2|^2W_{AB})R_{CB} \tag{3.49}$$

Putting these components together we find the unitary matrix describing our system is given by

$$U=\begin{pmatrix} r_1^*r_2^*e^{i\theta_1}R_{AB}W_{AB}R_{CB} & \tfrac{1}{t_1^*}(1-|r_1|^2W_{BA}) \\ R_{BC}\tfrac{1}{t_2}(-1+|r_2|^2W_{AB})R_{CB} & r_1r_2e^{i\theta_2}R_{BC}R_{BA}W_{BA} \end{pmatrix} \tag{3.50}$$

Constructing these diagrams is no more complicated than the Mach-Zehnder case but quite cumbersome. In the Mach-Zehnder case B entered further left than A and C and exited further right. In our current case B may enter from the left or right and exit from the left or right, meaning more diagrams of the form of Fig. 3.2 must be drawn. They are essentially of the same form where U and $U^\dagger$ of the 2-point case replace UV and $V^\dagger U^\dagger$ of the Mach-Zehnder case.

Since $|t_1|\sim|t_2|$ is small, higher order tunneling is exponentially suppressed. So we just quote the density matrices to order $|t|^2$ by a quicker method. Where the general form is the the same as the Mach-Zehnder case.

Firstly, we look at $U_{2,2}$ expanded to $n=1$, for the $S_\leftarrow$ case,

$$\begin{aligned} U_{2,2}U_{2,2}^\dagger &= \left(r_1r_2e^{i\theta_2}R_{BC}R_{BA}(1-t_1^*t_2e^{i(\theta_1+\theta_2)}R_{AB}R_{BA})\right) \\ &\times\left(r_1^*r_2^*e^{-i\theta_2}(1-t_1t_2^*e^{-i(\theta_1+\theta_2)}R_{AB}^{-1}R_{BA}^{-1})R_{AB}^{-1}R_{CB}^{-1}\right) \\ &= |r_1|^2|r_2|^2-|r_1|^2|r_2|^2t_1t_2^*e^{-i(\theta_1+\theta_2)}R_{BC}R_{BA}R_{AB}R_{BA}R_{AB}^{-1}R_{CB}^{-1} \\ &-|r_1|^2|r_2|^2t_1^*t_2e^{i(\theta_1+\theta_2)}R_{BC}R_{BA}R_{AB}^{-1}R_{BA}^{-1}R_{AB}^{-1}R_{CB}^{-1} \\ &+\underbrace{|r_1|^2|r_2|^2|t_1|^2|t_2|^2(\text{R-terms})}_{\sim t^4} \end{aligned} \tag{3.51}$$

through diagrammatic means we come to

$$\begin{aligned} p^{\rightarrow}_{aa'e,b} &\simeq |r_1|^2|r_2|^2\left(1 - t_1^* t_2 e^{i(\theta_1+\theta_2)} M_{ab} - t_1 t_2^* e^{-i(\theta_1+\theta_2)} M^*_{a'b}\right) \\ &\simeq 1 - |t_1|^2 - |t_2|^2 - |t_1 t_2| \left(e^{i\beta} M_{ab} + e^{-i\beta} M^*_{a'b}\right) \end{aligned} \tag{3.52}$$

Through the same method we can see that $U_{1,2}U^{\dagger}_{1,2}$, expanded to $n = 1$, gives

$$\begin{aligned} p^{\leftarrow}_{aa'e,b} &\simeq |t_1|^2 + |r_1|^2 t_1^* t_2 e^{i(\theta_1+\theta_2)} M_{ab} + |r_1|^2 t_1 t_2^* e^{-i(\theta_1+\theta_2)} M^*_{a'b} + |r_1|^4 |t_2|^2 M_{eb} \\ &\simeq |t_1|^2 + |t_1 t_2| \left(e^{i\beta} M_{ab} + e^{-i\beta} M^2_{a'b}\right) + |t_2|^2 M_{eb} \end{aligned} \tag{3.53}$$

where $\beta = arg\{t_1^* t_2 e^{i(\theta_1+\theta_2)}\}$. So, our probability is

$$p^{\rightarrow}_{aa'e,b} + p^{\leftarrow}_{aa'e,b} \simeq |t_2|^2 M_{eb} + |r_2|^2 \tag{3.54}$$

Again, taking the quantum trace of the target system, which projects on $e = 1$, so that $M_{eb} = 1$, gives us

$$p^{\rightarrow}_{aa'1,b} + p^{\leftarrow}_{aa'1,b} \simeq |t_2|^2 + |r_2|^2 = 1 \tag{3.55}$$

3.2.2 Reduced 3-point Gate Calculations

Since constructing the Unitary matrix for the 3-point poses a far greater problem than the 2-point gate we will begin by looking at three simplified special cases where we disallow tunnelling at each gate respectively, denoted by $|t_i| = 0$ ($\Rightarrow |r_i| = 1$). These will be useful in our full 3-point calculation. To further simplify matters we'll change notation so that a counter-clockwise rotation under the anyon A gives a phase $e^{i\theta_A}$ and over it gives $e^{i\theta'_A}$. Rotations around C give $e^{i\theta_C}$ and $e^{i\theta'_C}$ respectively. This also an interesting case to examine as, ideally, would would like to consider our gates to be switches that we can turn on and off to control the system.

$|t_3| = 0$: The first case is described by the diagrams where the transmission coefficient $|r_3| = 1$, since $|t_i|^2 + |r_i|^2 = 1$.

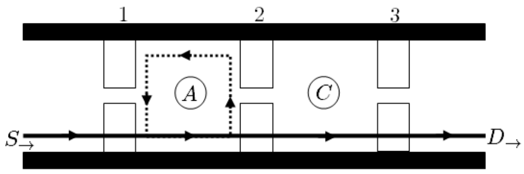

$$\Rightarrow r_1 r_2 e^{i(\theta_A+\theta_C)} R_{BC} R_{BA} W^{12}_{BA} \tag{3.56}$$

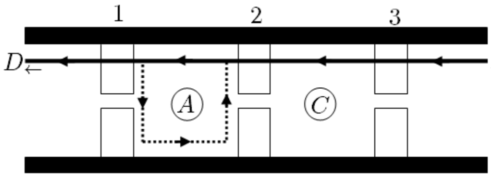

$$\Rightarrow r_1^* r_2^* e^{i(\theta'_A+\theta'_C)} R_{AB} W_{AB}^{12} R_{CB} \tag{3.57}$$

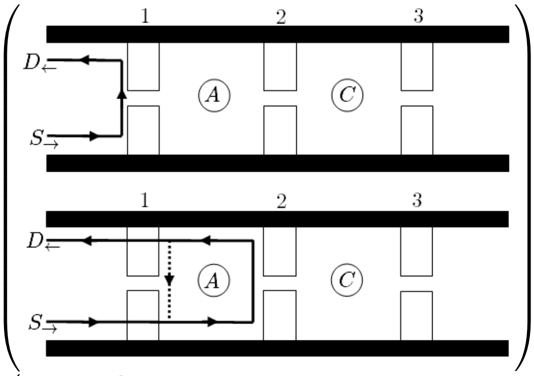

$$\Rightarrow \frac{1}{t_1^*}(1-|r_1|^2 W_{BA}^{12})$$

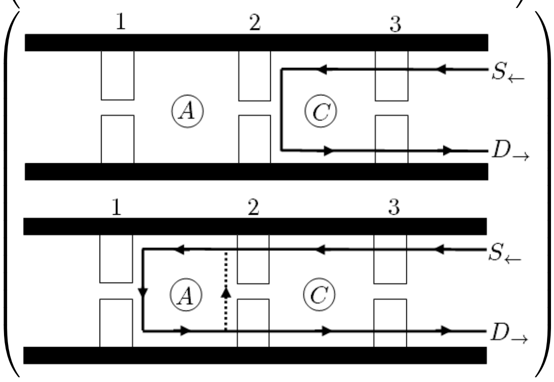

$$\Rightarrow \begin{array}{l} R_{BC}\frac{e^{i(\theta_C+\theta'_C)}}{t_2} \\ \times(-1+|r_2|^2 W_{AB}^{12})R_{CB} \end{array} \tag{3.58}$$

where we have defined a new wrapping term

$$W_{AB}^{12} := \sum_{n=0}^{\infty}\left(-t_1^* t_2 e^{i(\theta_A+\theta'_A)} R_{BA} R_{AB}\right)^n \tag{3.59}$$

The superscript indices (12) indicate which reflection coefficients are included. Since letting $t_3 = 0$ is almost equivalent to removing the third gate completely we see that we have almost exactly our 2-point gate and thus we get the same the Unitary matrix.

$$U_{|t_3|=0} = \begin{pmatrix} r_1^* r_2^* e^{i(\theta'_A+\theta'_C)} R_{AB} W_{AB}^{12} R_{CB} & \frac{1}{t_1^*}(1-|r_1|^2 W_{BA}^{12}) \\ R_{BC}\frac{e^{i(\theta_C+\theta'_C)}}{t_2}(-1+|r_2|^2 W_{AB}^{12})R_{CB} & r_1 r_2 e^{i(\theta_A+\theta_C)} R_{BC} R_{BA} W_{BA}^{12} \end{pmatrix} \tag{3.60}$$

The difference arises from the presence of the third gate. Looking back at Eq. 3.41 we see that we pick up a term $e^{i(\theta'_A)}$ but no term $e^{i(\theta'_C)}$, the only difference being the presence of the gate, which affects the phase regardless of whether tunneling takes place or not.

Which gives us, for the $S_{\leftarrow}$ case, up to $O(t^2)$,

$$\begin{aligned} p^{\rightarrow}_{aa'e,b} &\simeq |t_2|^2 + |t_1|^2|r_2|^2 + 2Re\{t_1 t_2^* e^{i(\theta'_A+\theta_A)} M_{ab}\}|r_2|^2 \\ &\simeq |t_2|^2 + |t_1|^2 + 2Re\{t_1 t_2^* e^{i(\theta'_A+\theta_A)} M_{ab}\} \\ p^{\leftarrow}_{aa'e,b} &\simeq |r_1|^2|r_2|^2 - 2Re\{t_1 t_2^* e^{i(\theta'_A+\theta_A)} M_{ab}\}|r_1|^2|r_2|^2 \\ &\simeq 1 - |t_2|^2 - |t_1|^2 - 2Re\{t_1 t_2^* e^{i(\theta'_A+\theta_A)} M_{ab}\} \end{aligned} \tag{3.61}$$

and we see that

$$p^{\rightarrow}_{aa'e,b} + p^{\leftarrow}_{aa'e,b} \simeq 1 \tag{3.62}$$

$|t_1| = 0$: We note that this case corresponds to nothing more than a relabelling of the previous case.

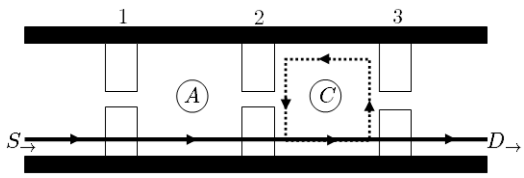

$$\Rightarrow r_2 r_3 e^{i\theta_C} R_{BC} W^{23}_{BC} R_{BA}$$

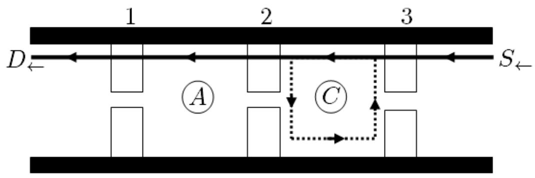

$$\Rightarrow r_2^* r_3^* e^{i\theta'_A+\theta'_C} R_{AB} W^{23}_{BC} R_{CB} \tag{3.63}$$

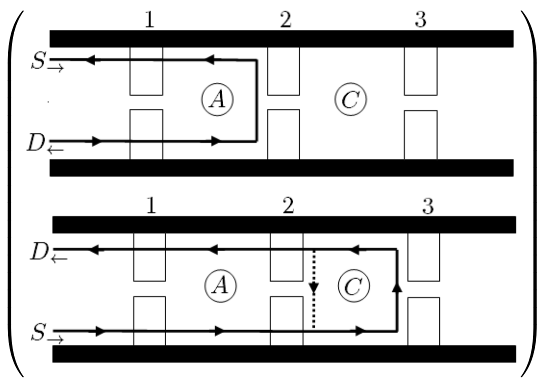

$$\Rightarrow \begin{array}{l} R_{AB} \frac{e^{i(\theta_A+\theta'_A)}}{t_2^*} \\ \times \left(1 - |r_2|^2 W^{23}_{BC}\right) R_{BA} \end{array} \tag{3.64}$$

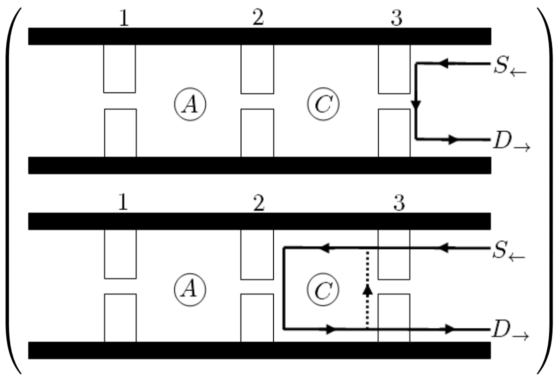

$$\Rightarrow \frac{1}{t_3}\left(-1+|r_2|^2 W^{23}_{CB}\right) \tag{3.65}$$

Where we have used

$$W^{23}_{BC} := \sum_{m=0}^{\infty}\left(-t_2^* t_3 e^{i(\theta_C+\theta'_C)} R_{CB} R_{BC}\right)^m \tag{3.66}$$

We find our Unitary matrix to be

$$U_{|t_1|=0} = \begin{pmatrix} r_2^* r_3^* e^{i\theta'_A+\theta'_C} R_{AB} W^{23}_{BC} R_{CB} & R_{AB}\frac{e^{i(\theta_A)+\theta'_A}}{t_2^*}\left(1-|r_2|^2 W^{23}_{BC}\right) R_{BA} \\ \\ \frac{1}{t_3}\left(-1+|r_2|^2 W^{23}_{CB}\right) & r_2 r_3 e^{i(\theta_A+\theta_C)} R_{BC} W^{23}_{BC} R_{BA} \end{pmatrix} \tag{3.67}$$

Which gives us, for the $S_{\leftarrow}$ case, up to $O(t^2)$,

$$\begin{aligned} p^{\leftarrow}_{cc'e,b} &\simeq 1-|t_2|^2-|t_3|^2-2Re\{t_2 t_3^* e^{i(\theta'_C+\theta_C)} M_{cb}\} \\ p^{\rightarrow}_{cc'e,b} &\simeq |t_2|^2+|t_3|^2+2Re\{t_2 t_3^* e^{i(\theta'_C+\theta_C)} M_{cb}\} \end{aligned} \tag{3.68}$$

$$p^{\rightarrow}_{cc'e,b}+p^{\leftarrow}_{cc'e,b} \simeq 1 \tag{3.69}$$

$|t_2| = 0$: Our final case is unique.

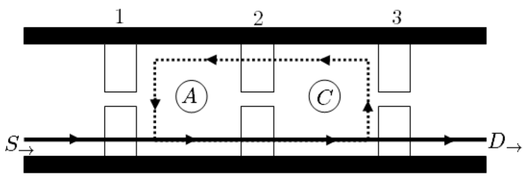

$$\Rightarrow r_1 r_3 e^{i(\theta_A+\theta_C)} W_{ABC} R_{BC} R_{BA} \tag{3.70}$$

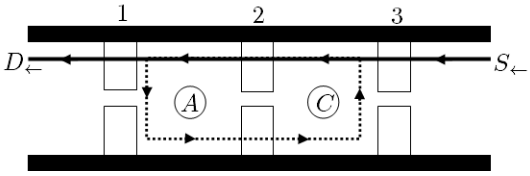

$$\Rightarrow r_1^* r_3^* e^{i(\theta'_A+\theta'_C)} W_{CBA} R_{AB} R_{CB} \tag{3.71}$$

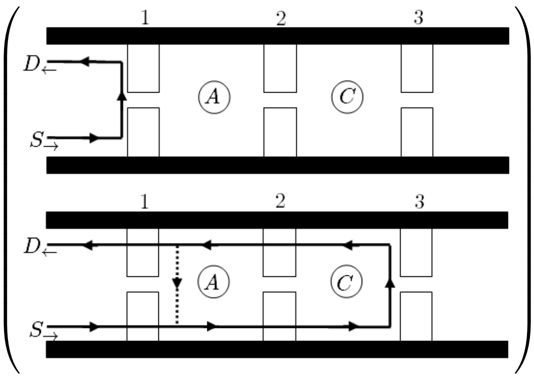

$$\Rightarrow \frac{1}{t_1^*}\left(1 - |r_1|^2 W_{CBA}\right) \tag{3.72}$$

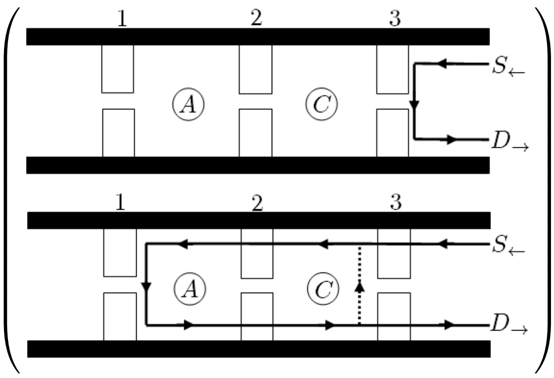

$$\Rightarrow \frac{1}{t_3}\left(-1 + |r_3|^2 W_{ABC}\right) \tag{3.73}$$

Where we have used new wrapping terms

$$W_{ABC} := \sum_{n=0}^{\infty}\left(-t_1^* t_3 e^{i(\theta_A + \theta'_A + \theta_C + \theta'_C)} R_{BC} R_{BA} R_{AB} R_{CB}\right)^n \tag{3.74}$$

$$W_{CBA} := \sum_{n=0}^{\infty}\left(-t_1^* t_3 e^{i(\theta_A + \theta'_A + \theta_C + \theta'_C)} R_{AB} R_{CB} R_{BC} R_{BA}\right)^n \tag{3.75}$$

Interestingly, we see that it is equivalent to treating A and C as a single particle.

$$U_{|t_2|=0} = \begin{pmatrix} r_1^* r_3^* e^{i(\theta'_A + \theta'_C)} W_{CBA} R_{AB} R_{CB} & \frac{1}{t_1^*}\left(1 - |r_1|^2 W_{CBA}\right) \\ \\ \frac{1}{t_3}\left(-1 + |r_3|^2 W_{ABC}\right) & r_1 r_3 e^{i(\theta_A + \theta_C)} W_{ABC} R_{BC} R_{BA} \end{pmatrix} \tag{3.76}$$

Which gives us, for the $S_{\leftarrow}$ case, up to $O(t^2)$,

$$
\begin{aligned}
p^{\leftarrow}_{aa'cc'e,b} &\simeq 1 - |t_1|^2 - |t_3|^2 - 2Re\{t_1 t_3^* e^{i(\theta'_A+\theta'_C+\theta_A+\theta_C)} M_{ab} M_{cb}\} \\
p^{\rightarrow}_{aa'cc'e,b} &\simeq |t_1|^2 + |t_3|^2 + 2Re\{t_1 t_3^* e^{i(\theta'_A+\theta'_C+\theta_A+\theta_C)} M_{ab} M_{cb}\}
\end{aligned}
\tag{3.77}
$$

$$
p^{\rightarrow}_{aa'cc'e,b} + p^{\leftarrow}_{aa'cc'e,b} \simeq 1 \tag{3.78}
$$

3.2.3 Full 3-point

We now consider the *"Full"* Unitary matrix up to $O(t^2)$. Where *Full* means that we consider all tunnelling gates to be turned on, we will not however attempt to construct the Unitary matrix for $n, t \to \infty$. Using the same method as before we find $U_{1,1}, U_{2,2} \sim \{1, t^2, t^4, ...\}$, and $U_{1,2}, U_{2,1} \sim \{t, t^3, t^5, ...\}$ as given below.

$$
\begin{aligned}
U_{1,1} = \ & r_1^* r_2^* r_3^* e^{i(\theta'_C+\theta'_A)} R_{AB} R_{CB} \\
& - r_1^* r_2^* r_3^* t_2^* t_3 e^{i(2\theta'_C+\theta'_A+\theta_C)} R_{AB} R_{CB} R_{BC} R_{CB} \\
& - r_1^* r_2^* r_3^* t_1^* t_2 e^{i(\theta'_C+2\theta'_A+\theta_A)} R_{AB} R_{BA} R_{AB} R_{CB} \\
& - r_1^* r_2^* r_3^* t_1^* t_3 |r_2|^2 e^{i(2\theta'_C+2\theta'_A+\theta_C+\theta_A)} R_{AB} R_{CB} R_{BC} R_{BA} R_{AB} R_{CB}
\end{aligned}
$$

$$
\begin{aligned}
U_{2,2} = \ & r_1 r_2 r_3 e^{i(\theta_C+\theta_A)} R_{BC} R_{BA} \\
& - r_1 r_2 r_3 t_2^* t_3 e^{i(\theta_{C'}+2\theta_C+\theta_A)} R_{BC} R_{CB} R_{BC} R_{BA} \\
& - r_1 r_2 r_3 t_1^* t_2 e^{i(\theta_C+\theta'_A+2\theta_A)} R_{BC} R_{BA} R_{AB} R_{BA} \\
& - r_1 r_2 r_3 t_1^* t_3 e^{i(\theta'_C+\theta'_A+2\theta_C+2\theta_A)} R_{BC} R_{BA} R_{AB} R_{CB} R_{BC} R_{BA}
\end{aligned}
$$

$$
\begin{aligned}
U_{1,2} = \ & t_1 \\
& + t_2 |r_1|^2 e^{i(\theta'_A+\theta_A)} R_{AB} R_{BA} \\
& + t_3 |r_1|^2 |r_2|^2 e^{i(\theta'_C+\theta'_A+\theta_C+\theta_A)} R_{AB} R_{CB} R_{BC} R_{BA}
\end{aligned}
\tag{3.79}
$$

$$
\begin{aligned}
U_{2,1} = \ & -t_3^* \\
& - t_2^* |r_3|^2 e^{i(\theta'_C+\theta_C)} R_{BC} R_{CB} \\
& - t_1^* |r_2|^2 |r_3|^2 e^{i(\theta'_C+\theta'_A+\theta_C+\theta_A)} R_{BC} R_{BA} R_{AB} R_{CB}
\end{aligned}
\tag{3.80}
$$

These terms can be checked by applying the three cases

$$
|t_i| = 0, \qquad |r_i| = 1, \qquad i = 1, 2, 3 \tag{3.81}
$$

and seeing that the resultant unitary matrices correspond to the simplified cases in Sec 3.2.2.

We note that up to $O(t^4)$ $U_{1,1}, U_{2,2}$ have eight extra terms each, and $U_{1,2}, U_{2,1}$ have four extra terms each.

Here we will just examine the $S_{\leftarrow}$ case. To make our calculation of $U_{1,1}U^{\dagger}_{1,1}$ easier, we consider $U_{1,1}$ to be

$$U_{1,1} = \alpha - \beta - \gamma - \delta \tag{3.82}$$

and $U^{\dagger}_{1,1}$ to be

$$U^{\dagger}_{1,1} = \alpha^{\dagger} - \beta^{\dagger} - \gamma^{\dagger} - \delta^{\dagger} \tag{3.83}$$

where $\beta, \delta, \gamma \sim O(t^2)$ so that we have

$$\begin{aligned} U_{1,1}U^{\dagger}_{1,1} = \alpha\alpha^{\dagger} \quad & -\alpha\beta^{\dagger} - \alpha\gamma^{\dagger} - \alpha\delta^{\dagger} \\ & -\beta\alpha^{\dagger} - \gamma\alpha^{\dagger} - \delta\alpha^{\dagger} \\ & +(\mathrm{O}(t^4)\mathrm{terms}) \end{aligned} \tag{3.84}$$

So we find

$$\begin{aligned} U_{1,1}U^{\dagger}_{1,1} \quad = & |r_1|^2|r_2|^2|r_3|^2 \\ & \times(1 - t_2t_3^{*}e^{-i(\theta'_C+\theta_C)}R_{AB}R_{CB}R^{-1}_{BC}R^{-1}_{CB}R^{-1}_{BC}R^{-1}_{BA} \\ & -t_1t_2^{*}e^{-i(\theta'_A+\theta_A)}R_{AB}R_{CB}R^{-1}_{BC}R^{-1}_{BA}R^{-1}_{AB}R^{-1}_{BA} \\ & -|r_2|^2t_1t_3^{*}e^{-i(\theta'_C+\theta_C+\theta'_A+\theta_A)}R_{AB}R_{CB}R^{-1}_{BC}R_{BA^{-1}}R^{-1}_{AB}R^{-1}_{CB}R^{-1}_{BC}R^{-1}_{BA} \\ & -t_2^{*}t_3e^{i(\theta'_C+\theta_C)}R_{AB}R_{CB}R_{BC}R_{CB}R^{-1}_{BC}R^{-1}_{BA} \\ & -t_1^{*}t_2e^{i(\theta'_A+\theta_A)}R_{AB}R_{BA}R_{AB}R_{CB}R^{-1}_{BC}R^{-1}_{BA} \\ & -|r_2|^2t_1^{*}t_3e^{i(\theta'_C+\theta'_A+\theta_C+\theta_A)}R_{AB}R_{CB}R_{BC}R_{BA}R_{AB}R_{CB}R^{-1}_{BC}R^{-1}_{BA}) \end{aligned} \tag{3.85}$$

Corresponding to the diagram $S_{\leftarrow}$ and $D_{\leftarrow}$ we have our equivalent of Eq.3.15

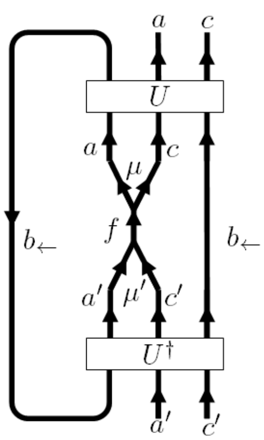

$$= \sum_{e,\alpha,\beta} [(F^{ac}_{a'c'})^{-1}]_{(f,\mu,\mu')(e,\alpha,\beta)}$$

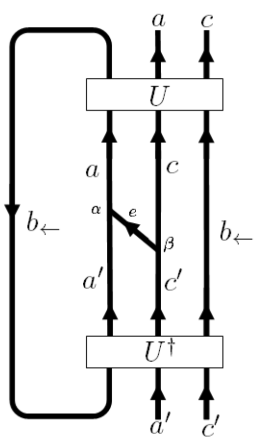

(3.86)

which gives us

$$= \sum_{e,\alpha,\beta} [(F^{ac}_{a'c'})^{-1}]_{(f,\mu,\mu')(e,\alpha,\beta)} |r_1|^2 |r_2|^2 |r_3|^2$$

$$\times \Bigg\{$$ 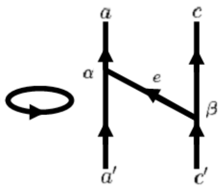 $$- t_2 t_3^* e^{-i(\theta'_C + \theta_C)}$$ 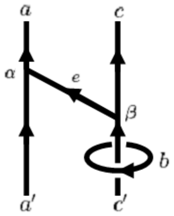 $$- t_1 t_2^* e^{-i(\theta'_A + \theta_A)}$$ 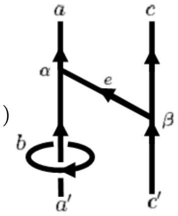

$$-|r_2|^2 t_1 t_3^* e^{-i(\theta'_C + \theta_C + \theta'_A + \theta_A)}$$ 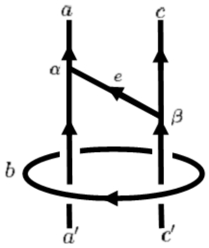 $$- t_2^* t_3 e^{i(\theta'_C + \theta_C)}$$ 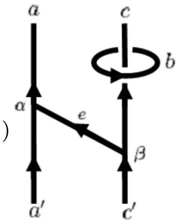

$$-t_1^* t_2 e^{i(\theta'_A + \theta_A)}$$ 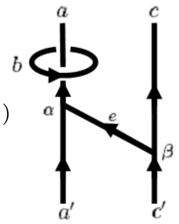 $$- |r_2|^2 t_1^* t_3 e^{i(\theta'_C + \theta'_A + \theta_C + \theta_A)}$$ 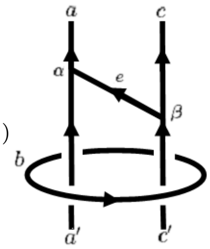 $$\Bigg\} \quad (3.87)$$

which leads us to

$$= d_b \sum_{e,\alpha,\beta} [(F^{ac}_{a'c'})^{-1}]_{(f,\mu,\mu')(e,\alpha,\beta)} |r_1|^2 |r_2|^2 |r_3|^2 \times$$

$$\begin{pmatrix} 1 - t_2 t_3^* e^{-i(\theta'_C + \theta_C)} M^*_{c'b} \\ -t_1 t_2^* e^{-i(\theta'_A + \theta_A)} M^*_{a'b} \\ -t_2^* t_3 e^{i(\theta'_C + \theta_C)} M_{cb} \\ -t_1^* t_2 e^{i(\theta'_A + \theta_A)} M_{ab} \\ -|r_2|^2 t_1 t_3^* e^{-i(\theta'_C + \theta_C + \theta'_A + \theta_A)} M^*_{ab} M^*_{cb} \\ -|r_2|^2 t_1^* t_3 e^{i(\theta'_C + \theta'_A + \theta_C + \theta_A)} M_{ab} M_{cb} \end{pmatrix} \times [F^{ac}_{a'c'}]_{(e,\alpha,\beta)(f',\nu,\nu')}$$ 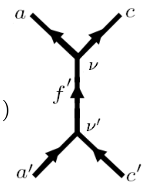

$$(3.88)$$

gives us

$$= d_b \sum_{\substack{e,\alpha,\beta \\ f',\nu,\nu'}} [(F^{ac}_{a'c'})^{-1}]_{(f,\mu,\mu')(e,\alpha,\beta)} [F^{ac}_{a'c'}]_{(e,\alpha,\beta)(f',\nu,\nu')} p^{\leftarrow}_{aa'cc'e,b}$$ 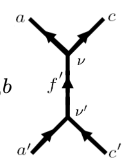 $$(3.89)$$

where

$$
\begin{aligned}
p^{\leftarrow}_{aa'cc'e,b} \simeq |r_1|^2|r_2|^2|r_3|^2 \quad & -t_2t_3^*|r_1|^2|r_2|^2|r_3|^2e^{-i(\theta'_C+\theta_C)}M^*_{c'b} \\
& -t_1t_2^*|r_1|^2|r_2|^2|r_3|^2e^{-i(\theta'_A+\theta_A)}M^*_{a'b} \\
& -t_2^*t_3|r_1|^2|r_2|^2|r_3|^2e^{i(\theta'_C+\theta_C)}M_{cb} \\
& -t_1^*t_2|r_1|^2|r_2|^2|r_3|^2e^{i(\theta'_A+\theta_A)}M_{ab} \\
& -t_1t_3^*|r_1|^2|r_2|^4|r_3|^2e^{-i(\theta'_C+\theta_C+\theta'_A+\theta_A)}M^*_{ab}M^*_{cb} \\
& -t_1^*t_3|r_1|^2|r_2|^4|r_3|^2e^{i(\theta'_C+\theta'_A+\theta_C+\theta_A)}M_{ab}M_{cb}
\end{aligned} \tag{3.90}
$$

$$
\simeq \begin{pmatrix} 1-|t_1|^2-|t_2|^2-|t_3|^2 \\ -2Re\{t_2t_3^*e^{i(\theta'_C+\theta_C)}M_{cb}\} \\ -2Re\{t_1t_2^*e^{i(\theta'_A+\theta_A)}M_{ab}\} \\ -2Re\{t_1t_3^*e^{i(\theta'_C+\theta'_A+\theta_C+\theta_A)}\} \end{pmatrix} \tag{3.91}
$$

We now look at $U_{2,1}U^{\dagger}_{2,1}$, which corresponds to the $S_{\leftarrow}$ and $D_{\rightarrow}$ case,

$$
\begin{aligned}
U_{2,1}U^{\dagger}_{2,1} = |t_3|^2 \quad & +t_2t_3^*|r_3|^2e^{-i(\theta'_C+\theta_C)}R^{-1}_{BC}R^{-1}_{CB} \\
& +t_1t_3^*|r_2|^2|r_3|^2e^{-i(\theta'_C+\theta'_A+\theta_C+\theta_A)}R^{-1}_{BC}R^{-1}_{BA}R^{-1}_{AB}R^{-1}_{CB} \\
& +t_2^*t_3|r_3|^2e^{i(\theta'_C+\theta_C)}R_{BC}R_{CB} \\
& +|t_2|^2|r_3|^4R_{BC}R_{CB}R^{-1}_{BC}R^{-1}_{CB} \\
& +t_1t_2^*|r_2|^2|r_3|^4e^{-i(\theta'_A+\theta_A)}R_{BC}R_{CB}R^{-1}_{BC}R^{-1}_{BA}R^{-1}_{AB}R^{-1}_{CB} \\
& +t_1^*t_3|r_2|^2|r_3|^2e^{i(\theta'_C+\theta'_A+\theta_C+\theta_A)}R_{BC}R_{BA}R_{AB}R_{CB} \\
& +t_1^*t_2|r_2|^2|r_2|^4e^{i(\theta'_A+\theta_A)}R_{BC}R_{BA}R_{AB}R_{CB}R^{-1}_{BC}R^{-1}_{CB} \\
& +|t_1|^2|r_2|^2|r_3|^2R_{BC}R_{BA}R_{AB}R_{CB}R^{-1}_{BC}R^{-1}_{BA}R^{-1}_{AB}R^{-1}_{CB}
\end{aligned} \tag{3.92}
$$

Similar to $U_{1,1}$ we have

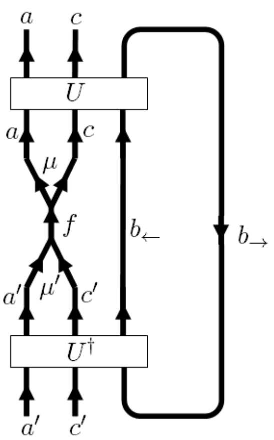

$$= \sum_{e,\alpha,\beta} [(F^{ac}_{a'c'})^{-1}]_{(f,\mu,\mu')(e,\alpha,\beta)}$$

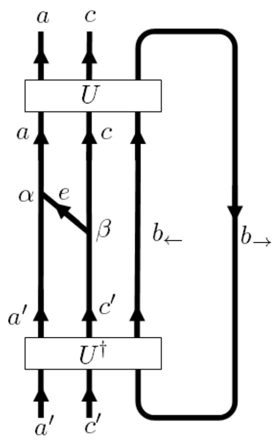

(3.93)

which gives us

$$= \sum_{e,\alpha,\beta} [(F^{ac}_{a'c'})^{-1}]_{(f,\mu,\mu')(e,\alpha,\beta)}$$

$$\times \Bigg\{ |t_3|^2$$

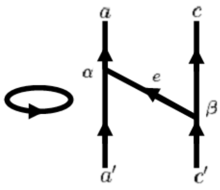

$$+ t_2 t_3^* |r_3|^2 e^{-i(\theta'_C + \theta_C)}$$

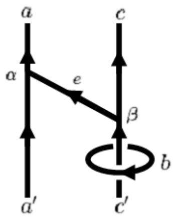

$$+ t_1 t_3^* |r_2|^2 |r_3|^2 e^{-i(\theta'_C + \theta'_A + \theta_C + \theta_A)}$$

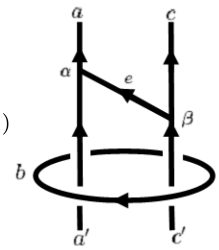

$$+ t_2^* t_3 |r_3|^2 e^{i(\theta'_C + \theta_C)}$$

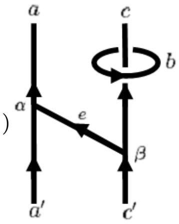

$$+ |t_2|^2 |r_3|^4$$

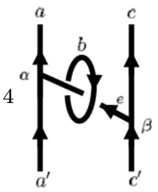

$$+ t_1 t_2^* |r_2|^2 |r_3|^4 e^{-i(\theta'_A + \theta_A)}$$

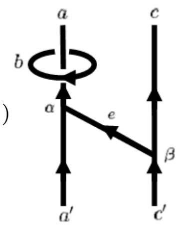

$$+ t_1^* t_3 |r_2|^2 |r_3|^2 e^{i(\theta'_C + \theta'_A + \theta_C + \theta_A)}$$

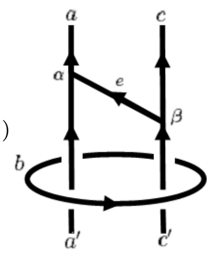

$$+ t_1^* t_2 |r_2|^2 |r_2|^4 e^{i(\theta'_A + \theta_A)}$$

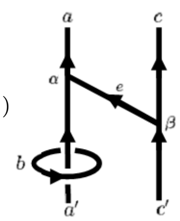

$$+ |t_1|^2 |r_2|^2 |r_3|^2$$

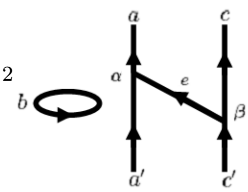

$$\Bigg\} \tag{3.94}$$

and we get

$$= d_b \sum_{e,\alpha,\beta} [(F^{ac}_{a'c'})^{-1}]_{(f,\mu,\mu')(e,\alpha,\beta)} \times$$

$$\begin{pmatrix} |t_3|^2 + t_2 t_3^* |r_3|^2 e^{-i(\theta'_C + \theta_C)} M^*_{c'b} \\ + t_1 t_3^* |r_2|^2 |r_3|^2 e^{-i(\theta'_C + \theta'_A + \theta_C + \theta_A)} M_{a'b} M_{b'c} \\ + t_2^* t_3 |r_3|^2 e^{i(\theta'_C + \theta_C)} M_{cb} \\ + |t_2|^2 |r_3|^4 M_{eb} \\ + t_1 t_2^* |r_2|^2 |r_3|^4 e^{-i(\theta'_A + \theta_A)} M_{ab} \\ + t_1^* t_3 |r_2|^2 |r_3|^2 e^{i(\theta'_C + \theta'_A + \theta_C + \theta_A)} M_{ab} M_{cb} \\ + t_1^* t_2 |r_2|^2 |r_3|^4 e^{i(\theta'_A + \theta_A)} M_{a'b} \\ + |t_1|^2 |r_2|^2 |r_3|^2 \end{pmatrix} \times [F^{ac}_{a'c'}]_{(e,\alpha,\beta)(f',\nu,\nu')} \tag{3.95}$$

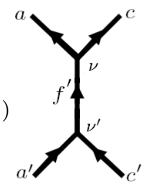

gives us

$$= d_b \sum_{\substack{e,\alpha,\beta \\ f',\nu,\nu'}} [(F^{ac}_{a'c'})^{-1}]_{(f,\mu,\mu')(e,\alpha,\beta)} [F^{ac}_{a'c'}]_{(e,\alpha,\beta)(f',\nu,\nu')} p^{\rightarrow}_{aa'cc'e,b} \tag{3.96}$$

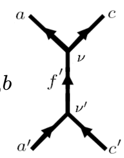

where we have defined

$$\begin{aligned} p^{\rightarrow}_{aa'cc'e,b} \simeq |t_3|^2 \quad & + t_2 t_3^* |r_3|^2 e^{-i(\theta'_C + \theta_C)} M^*_{c'b} \\ & + t_1 t_3^* |r_2|^2 |r_3|^2 e^{-i(\theta'_C + \theta'_A + \theta_C + \theta_A)} M_{a'b} M_{c'b} \\ & + t_2^* t_3 |r_3|^2 e^{i(\theta'_C + \theta_C)} M_{cb} \\ & + |t_2|^2 |r_3|^4 M_{eb} \\ & + t_1 t_2^* |r_2|^2 |r_3|^4 e^{-i(\theta'_A + \theta_A)} M_{ab} \\ & + t_1^* t_3 |r_2|^2 |r_3|^2 e^{i(\theta'_C + \theta'_A + \theta_C + \theta_A)} M_{ab} M_{cb} \\ & + t_1^* t_2 |r_2|^2 |r_3|^4 e^{i(\theta'_A + \theta_A)} M_{a'b} \\ & + |t_1|^2 |r_2|^2 |r_3|^2 \end{aligned} \tag{3.97}$$

$$\simeq \begin{pmatrix} |t_1|^2 + |t_2|^2 M_{eb} + |t_3|^2 \\ + 2Re\{t_2 t_3^* e^{i(\theta'_C + \theta_C)} M_{cb}\} \\ + 2Re\{t_1 t_2^* e^{i(\theta'_A + \theta_A)} M_{ab}\} \\ + 2Re\{t_1 t_3^* e^{i(\theta'_C + \theta'_A + \theta_C + \theta_A)} M_{ab} M_{cb}\} \end{pmatrix} \tag{3.98}$$

Again, these terms can be checked by applying the three cases

$$|t_i| = 0, \qquad |r_i| = 1, \qquad i = 1, 2, 3 \tag{3.99}$$

and seeing that the resultant density matrices correspond to the simplified cases in Sec 3.2.2.

So we see that

$$p^{\leftarrow}_{aa'cc'e,b} + p^{\rightarrow}_{aa'cc'e,b} \simeq |t_2|^2 M_{eb} + |r_2|^2 \tag{3.100}$$

which is exactly the result for the 2-point gate. Again, taking the quantum trace of the target system, which projects on $e = 1$, so that $M_{eb} = 1$, gives us a well defined probability distribution

$$p^{\leftarrow}_{aa'cc'e,b} + p^{\rightarrow}_{aa'cc'e,b} \simeq |t_2|^2 + |r_2|^2 = 1 \tag{3.101}$$

3.3 Further Analysis

Further analysis could include constructing a complete unitary matrix for the 3-point Fabry-Pérot to all orders.

Having the complete unitary matrix would allow us to study other interesting cases such as

$$|t_i| \simeq |t_j|, \quad |t_k| \simeq 0, \qquad i,j,k = 1,2,3, \qquad i \neq j \neq k \tag{3.102}$$

Which is the case where one of the tunneling amplitudes is much weaker than the other two. This would allow us to approximate the situation with 3 gates, where one is turned 'off', but allowing for the possibility that tunneling may occur at the off gate, and compare it with the situation

$$|t_i| \simeq |t_j|, \quad |t_k| = 0, \qquad i,j,k = 1,2,3, \qquad i \neq j \neq k \tag{3.103}$$

where one of the gates is completely off.

Another interesting case is

$$|t_i| \to 1, \quad |t_k| \simeq |t_j| \simeq 0, \qquad i,j,k = 1,2,3, \qquad i \neq j \neq k \tag{3.104}$$

Where we consider one of the gates to have much higher tunneling than the other two, and allowing the stronger amplitude to approach 1.

We may also like to some of the apply specific anyon models (Fibonacci, Ising, etc) discussed in [4] to the complete case to see if it leads to any interesting results.

Bibliography

[1] M. Nielson and I. Chuang,
Quantum Computation and Quantum Information
(Cambridge Press, 2000).

[2] J.Gruska,
Quantum Computing
(McGraw-Hill Publishing company, ISBN 007 709503 0, 1999).

[3] P.Bonderson, K.Shtengel, and J.Slingerland,
Interferometry of Non-Abelian Anyons
(arXiv: 0707.4206v2[quant-ph], 2008).

[4] P.Bonderson,
Non-Abelian anyons and interferometry
(http://etd.caltech.edu/etd/available/etd-06042007-101617/, 2007).

[5] S. DasSarma, M.Freedman, and C.Nayak,
Topologically-Protected Qubits from a Possible Non-Abelian Fractional Quantum Hall State
(arXiv: [cond-mat] 0412343v2, 2008).

[6] Nayak, Simon, Freedman, Stern, and DasSarma,
Non-Abelian Anyons and Topological Quantum Computation
(arXiv:0707.1889v2 [cond-mat.str-el], 2008).

[7] E. Hall,
On a New Action of the Magnet on Electric Currents
(American Journal of Mathematics vol 2, p.287-292, 1879).

[8] T. Ando, Y. Matsumoto, and Y. Uemura,
Theory of Hall Effect in a Two-Dimensional Electron System
(J. Phys. Soc. Jpn. 39 pp. 279-288, 1975).

[9] R. B. Laughlin,
Quantized Hall conductivity in two dimensions
(Phys. Rev. B 23, 5632 - 5633, 1981).

[10] K. V. Klitzing, G. Dorda, and M. Pepper,
New Method for High-Accuracy Determination of the Fine-Structure Con-

stant Based on Quantized Hall Resistance
(Phys. Rev. Lett. 45, 494 - 497, 1980).

[11] K.S.Novoselov *et al.*,
Room-Temperature Quantum Hall Effect in Graphene
(Science DOI: 10.1126/science.1137201, 2007).

[12] J.P.Eisenstein and H.L.Stormer,
The Fractional Quantum Hall Effect
(science, 248 (4962):1510-1516, 1990).

[13] L. D. Landau,
Diamagnetism of Metals
(Z. Phys. 64, 629, 1930).

[14] P.Bonderson and J.K.Slingerland,
Fractional Quantum Hall Hierarchy and the Second Landau Level
(ArXiv:0711.3204v3 [cond-mat.mes-hall], 2008).

[15] J.K.Slingerland,
Quantum Hall trial wave functions and CFT
(www.stp.dias.ie/∼slingerland/Halllect/halllecture1.pdf, 2002).

[16] B.L.Johson and G.Kirczenow,
Composite Fermions in the Quantum Hall Effect
(Rep. Prog. Phys. 60, 889-939, 1996).

[17] R. B. Laughlin,
Anomalous quantum hall effect: an incompressible fluid with fractionally charge statistics
(Phys. Rev. Lett., 50:1395, 1983).

[18] F.D.M.Haldane,
Fractional Quantization of the Hall Effect: A Hierarchy of Incompressible Quantum Fluid States
(Phys. Rev. Lett. 51, 605, 1983).

[19] B.I.Halperin,
Statistics of Quasiparticles and the Hierarchy of Fractional Quantized Hall States
(Phys. Rev. Lett. 52, 1583, 1984).

[20] H.L.Stormer *et al.*,
Fractional Quantization of the Hall Effect
(Phys. Rev. Lett. 50, 1953, 1983).

[21] D.C.Tsui, H.L.Stormer, and A.C.Gossard,
Two-Dimensional Magnetotransport in the Extreme Quantum Limit
(Phys. Rev. Lett. 48, 1559, 1982).

[22] H.L.Stormer *et al.*,
Observation of an even-denominator quantum number in the fractional quantum Hall effect
(Phys. Rev. Lett. 59, 1776, 1987).

[23] G.Moore and N.Read,
Nonabelions in the fractional quantum Hall effect
(Nucl. Phys. B 360(2-3),362, 1991).

[24] Leinaas and J.Myrheim,
On the theory of Identical Particles
(Il Nuovo Cimento B 37 (1): 1-23. doi:10.1007/BF02727953, 1977).

[25] V. Lahtinan,
Anyons, Quantum Double Symmetry and Topological Quantum Computation
(URN:NBN:fi-fe20061380, 2006).

[26] C.Montonen,
The Many-Anyon Problem
(quant-ph/9502071, 1994).

[27] J. C.Baez,
Braids and Quantization: Rambling Lectures by John C.Baez
(http://math.ucr.edu/home/baez/braids/, 1992).

[28] L.Kauffman,
Knots and Physics
(World Scientific, 1991).

[29] Yu.I.Manin,
Quantum Groups and Noncommutative Geometry
(Centre De Recherches Mathema, 1988).

[30] A.Kitaev,
Anyons in exactly solved models and beyond
(Annual of Physics.321, 2-111 cond-mat/0506438, 2006).

[31] J.Preskill,
Topological Quantum Computation, Lecture notes
(http://www.theory.caltech.edu/∼preskill/, 2004).

[32] P. Bonderson, K. Shtengel, and J.K.Slingerland,
Probing Non-Abelian Statistics with Quasiparticle Interferometry
(arXiv: [cond-mat] 0601242v3, 2006).

[33] L.Mach,
Uber einer Interferenzrefractor
(Zeitschr. f. Instrkde. 12 89-93, 1892).

[34] L.Zehnder,
Ein neuer Interferenzrefractor
(Zeitschr. f. Instrkde. 11 275-285, 1891).

[35] M.Peshkin and A.Tonomura,
The Aharonov-Bohm effect
(Springer-Verlag. ISBN 3-540-51567-4, 1989).

[36] Y.Wu, Y.Hatsugai, and M.Kohmoto,
Anyons on a torus: Braid group, Aharonov-Bohm period, and numerical study
(Phys.Rev., Vol.43, No.13, 1991).

[37] G.Hernandez,
FabryPérot Interferometers
(Cambridge University Press. ISBN 0521322383, 1986).

[38] S.DasSarma, R.deSousa, X.Hu, and B.Koiller,
Spin quantum computation in silicon nanostructures
(arXiv:cond-mat/0411755v1 [cond-mat.mes-hall], 2004).

[39] Chamon, Freed, Kivelson, Sondhi, and Wen,
Two point-contact interferometer for quantum hall systems
(Phys. Rev.B 55,2331-43, 1997).